Bone Morphogenetic Protein and Retinoic Acid Synergistically Specify Female Germ Cell Fate in Mice

Hidetaka Miyauchi,[1,2] Hiroshi Ohta,[1,2] So Nagaoka,[1,2] Fumio Nakaki,[1,2] Kotaro Sasaki,[1,2] Katsuhiko Hayashi,[1,3,4] Yukihiro Yabuta,[1,2] Tomonori Nakamura,[1,2] Takuya Yamamoto,[5,6,7] and Mitinori Saitou.[1,2,5,6,8]

[1]Department of Anatomy and Cell Biology, Graduate School of Medicine, Kyoto University, Yoshida-Konoe-cho, Sakyo-ku, Kyoto 606-8501, Japan.
[2]JST, ERATO, Yoshida-Konoe-cho, Sakyo-ku, Kyoto 606-8501, Japan.
[3]JST, PRESTO, Maidashi 3-1-1, Higashi-ku, Fukuoka 812-8582, Japan.
[4]Department of Developmental Stem Cell Biology, Faculty of Medical Sciences, Kyushu University, Maidashi 3-1-1, Higashi-ku, Fukuoka 812-8582, Japan.
[5]Center for iPS Cell Research and Application, Kyoto University, 53 Kawahara-cho, Shogoin, Sakyo-ku, Kyoto 606-8507, Japan.
[6]Institute for Integrated Cell-Material Sciences, Kyoto University, Yoshida-Ushinomiya-cho, Sakyo-ku, Kyoto 606-8501, Japan.
[7]AMED-CREST, AMED, 1-7-1 Otemachi, Chiyoda-ku, Tokyo, 100-0004, Japan.
[8]Lead Contact

Running title: BMP and RA Specify Female Germ Cell Fate

**Correspondence should be addressed to:*
Mitinori Saitou, M.D., Ph.D.
E-mail:saitou@anat2.med.kyoto-u.ac.jp
Tel: +81-75-753-4335; Fax: +81-75-751-7286 (MS)

SUMMARY

The mechanism for sex determination in mammalian germ cells remains unclear. Here, we establish an in vitro reconstitution of female sex determination in mouse germ cells under a defined condition without the use of gonadal somatic cells. We show that retinoic acid (RA) and its key effector, STRA8, are not sufficient to induce the female germ-cell fate. In contrast, bone morphogenetic protein (BMP) and RA synergistically induce primordial germ cells (PGCs)/PGC-like cells (PGCLCs) derived from embryonic stem cells (ESCs) into fetal primary oocytes. Such induction, characterized by the entry into the meiotic prophase, occurs synchronously, recapitulates in vivo cytological and transcriptome progression faithfully, and necessitates a proper cellular competence, most typically, DNA demethylation of relevant genes, which is manifested by PGCs/PGCLCs propagated appropriately, but not by PGCs/PGCLCs immediately after induction. Our findings provide a framework for a comprehensive delineation of the sex determination pathway in mammalian germ cells, including humans.

HIGHLIGHTS

1. Female mouse germ-cell sex determination is reconstituted under a defined condition.

2. Retinoic acid (RA) and STRA8 are not sufficient to induce the female germ-cell fate.

3. Bone morphogenetic protein (BMP) and RA synergistically induce female germ-cell fate.

4. Competence for the female germ-cell fate includes DNA demethylation of key genes.

INTRODUCTION

In multicellular organisms, which are typically diploids, the germ cell lineage undergoes sexually dimorphic development and ensures sexual reproduction. A key event that underpins sexual reproduction is the meiosis, which shuffles parental chromosomes after their replication through meiotic recombination and generates haploid gametes with novel genetic constitutions via successive reduction divisions (Baudat et al., 2013; Handel and Schimenti, 2010). The fusion, or fertilization, of the resultant gametes from both sexes, the spermatozoa and the oocytes, leads to the formation of diploid zygotes, resulting in the creation of a potentially enormous level of genetic diversity. Therefore, improved understanding of the mechanism for sexual differentiation of germ cells, including meiosis, would provide essential information not only in regard to the mechanisms by which genetic diversity and organismal evolution are generated, but also in regard to the diseased states arising from anomalies in these processes.

The germ cell lineage in mice is induced in the epiblast by signaling molecules and is established as primordial germ cells (PGCs) at around embryonic day (E) 7.25 (Lawson et al., 1999; Ohinata et al., 2009; Saitou et al., 2002). PGCs undergo migration and colonize embryonic gonads from around E10.5, while exhibiting rapid proliferation and epigenetic reprogramming including genome-wide DNA demethylation (Kagiwada et al., 2013; Seisenberger et al., 2012). During this period, PGCs are sexually uncommitted, and their sexual fates are determined, not by their chromosomal sexes *per se*, but by signals/environmental effects from embryonic gonads: In XY males, the Y-chromosome-encoded gene, *Sry*, initiates transcriptional cascades specifying indifferent gonads into testes at around E10.5, while in XX females, the lack of *Sry* leads to the formation of ovaries (Lin and Capel, 2015). Consequently, after around E13.5, XY PGCs in the embryonic testes enter into mitotic arrest to differentiate into pro-spermatogonia (PSG), whereas XX PGCs in the embryonic ovaries progress into meiosis to differentiate into primary oocytes (Spiller and Bowles, 2015). Accordingly, it has been shown that retinoic acid (RA), apparently synthesized primarily in the mesonephric ducts, induces XX PGCs in embryonic ovaries into the female pathway by up-regulating the expression of STRA8, a molecule essential for triggering the meiotic prophase, whereas in embryonic testes, RA is degraded by CYP26B1 strongly expressed in nascent Sertoli cells and XY PGCs ensheathed by such cells are induced into the male pathway via an as-yet-unknown mechanism (Bowles et al., 2006; Koubova et al., 2006; Spiller and Bowles, 2015).

The pursuit of a more detailed understanding of the mechanism for sexual determination of germ cells, however, has been protracted. As to the female pathway, critical questions such as whether RA is sufficient for the female germ-cell fate or other signaling pathways are necessary, and which transcription factor(s) may drive the pre-meiotic DNA replication remain unresolved. This is in part due to the difficulty in analyzing complex

interactions between germ cells and gonadal somatic cells and the lack of an in vitro system amenable for assessing the relevant processes in a constructive fashion. On the other hand, it has been shown that mouse embryonic stem cells (ESCs)/induced pluripotent stem cells (iPSCs) are induced into epiblast-like cells (EpiLCs), which are in turn induced into PGC-like cells (PGCLCs) with characteristics of migrating PGCs. Importantly, PGCLCs bear a robust capacity both for spermatogenesis and oogenesis, upon transplantation or aggregation with gonadal somatic cells followed by appropriate culture (Hayashi et al., 2012; Hayashi et al., 2011; Hikabe et al., 2016; Ishikura et al., 2016; Saitou and Miyauchi, 2016). More recently, a system that allows the propagation of PGCLCs, at least for a week, without the use of gonadal somatic cells has been developed, creating an opportunity to reconstitute the sex determination pathway of germ cells under a defined condition in vitro (Ohta et al., 2017). We here explore this possibility with a focus on the female pathway and delineate a framework for the determination of female germ-cell fate.

RESULTS

A System for Analyzing the Sex-Determination Mechanism of Germ Cells

We have recently developed a system to propagate PGCLCs up to ~50-fold during a 7-day culture in the presence of stem cell factor (SCF) and the stimulators of cAMP signaling, Forskolin and Rolipram, on m220 feeders (Figure 1A) (Ohta et al., 2017). Under this condition, PGCLCs maintain their transcriptome as migrating/early gonadal PGCs, which are sexually uncommitted, while progressively erasing their DNA methylome to acquire genome-wide DNA methylation levels (~5%) and patterns equivalent to those in germ cells at E13.5, which are committed either to the male or the female fate (Saitou and Miyauchi, 2016; Spiller and Bowles, 2015). These findings indicate that DNA methylation reprogramming and sexual differentiation in germ cells are genetically separable and that PGCLCs cultured under this condition may serve as an appropriate system to explore the mechanisms for sexual differentiation of germ cells.

We here examined this possibility with a focus on differentiation into the female pathway, which is characterized by the entry into meiotic prophase. We reasoned that one prerequisite of the differentiation of PGCLCs into the female pathway is their acquisition of late PGC properties, typically characterized by the expression of genes such as *Dazl* and *Ddx4* [also known as *mouse vasa homolog* (*mVH*)], both of which are expressed at low levels in PGCLCs and show progressive up-regulation in PGCs/germ cells up to E13.5 (Figure 1A) (Cooke et al., 1996; Fujiwara et al., 1994; Kagiwada et al., 2013; Ohta et al., 2017). Moreover, *Dazl* has been proposed to act as a "licensing" factor for the sexual differentiation of germ cells (Gill et al., 2011; Lin et al., 2008). We generated ESC lines expressing *mVenus*, *ECFP*, and *tdTomato* or *RFP* under the control of *Blimp1* (also known as *Prdm1*), *Stella* (also known as *Dppa3*), and *Dazl* or *Ddx4* (mVH), respectively [*Blimp1-mVenus*:*Stella-ECFP*:*Dazl-tdTomato* (BVSCDT) or BVSC:*mVH-RFP* (BVSCVR), respectively] (Figure S1A-E) **[EXPERIMENTAL PROCEDURES]** (Imamura et al., 2010), and attempted to establish a condition for driving DT or VR expression in cultured PGCLCs followed by/coupled with their entry into the female fate and down-regulation of BVSC expression. Since both XY and XX germ cells can take on the female fate (Evans et al., 1977; Taketo, 2015), we used both XY and XX ESCs as starting materials, which gave essentially the same results (see below).

We induced BVSCDT ESCs (XY) into PGCLCs and isolated BV-positive (+) day (d) 4 PGCLCs by fluorescence activated cell sorting (FACS) for the expansion culture. At culture day 3 (c3), by which time point the PGCLCs were propagating exponentially, we provided the culture with a panel of cytokines that might have an impact on sex determination in the absence or presence (100 nM) of RA, and at c7, evaluated their effects on BV/DT expression by FACS (Figure 1A, B). Consistent with our recent report (Ohta et al., 2017), under the control condition (no additional cytokines and no RA), BV (+) c7 PGCLCs showed, on average, relatively low DT expression (Figure 1B, C).

Interestingly, the addition of RA elevated the DT levels in the BV (+) cell population (Figure 1B, C). Notably, combined addition of RA and one of the ligands of the bone morphogenetic protein family (BMP2, 4, 5 and 7), but not any of the other cytokines examined, strongly activated DT and, concomitantly, down-regulated BV (Figure 1B), suggesting that RA and BMP induced PGCLCs into late PGC-like cells or an even further-differentiated phenotype.

Among the BMP ligands, *Bmp2* is expressed strongly in response to a key feminizing factor, *Wnt4*, in pre-granulosa cells that would direct the female germ-cell fate (Figure S1F) (Jameson et al., 2012; Yao et al., 2004). Next, therefore, we examined the effects of RA and BMP2 on the expression of BVSCVR in cultured PGCLCs induced from BVSCVR ESCs (XX). We cultured BV (+) d4 PGCLCs, provided varying concentrations of RA and BMP2 at c3, and examined their effects on BVSCVR expression at c9 (Figure 1A, D). As shown in Figure 1D, RA alone (100 nM) did not significantly change the BVSC expression and did not activate VR, suggesting a differential regulation between *Dazl* and *Ddx4* expression. In contrast, remarkably, combined addition of RA and BMP2 induced BVSC down-regulation and robust VR up-regulation, and the percentage of the induction of the VR (+) cells increased in a BMP dose-dependent fashion (Figure 1D). Interestingly, we found that BMP2 alone (300 ng/ml) down-regulated BV and activated VR (see below), and the extent of BVSC down-regulation and VR activation increased in an RA dose-dependent fashion (Figure 1E).

By immunofluorescence (IF) analysis, we examined the expression of DDX4 and SCP3 (also known as SYCP3), a key component of the synaptonemal complex and a marker for meiotic prophase (Yuan et al., 2000), in cultured PGCLCs with RA (100 nM) and BMP2 (300 ng/ml) at c9 [induced from BVSC ESCs (XX)]. The results showed that the BV/SC (+) cells detected by anti-EGFP antibody staining expressed DDX4 and SCP3 in a manner highly similar to E15.5 primary oocytes: DDX4 exhibited specific localization at the cytoplasm and SCP3 showed distinct localization indicative of the synaptonemal complex formation, while DDX4/SCP3 (+) cells appeared to be interconnected, reminiscent of the formation of ovarian cysts (Figure 1G) (Pepling and Spradling, 1998). When combined with RA, the other BMP ligands (BMP4, 5, 7) were also capable of inducing VR/DDX4 and SCP3 (+) cells (Figure S1G, H). These findings indicate the possibility that the combined action of RA and BMP signaling leads cultured PGCLCs into the female pathway.

BMP and RA Commit PGCLCs to the Female Fate

We went on to explore the effect of RA and BMP signaling on PGCLCs induced from BVSCVR ESCs (XX) in a more detailed fashion. We confirmed that although the culture with RA from c3 onwards slightly down-regulated BV and elevated SC, it did not induce

VR by c9 (Figure 2A). In contrast, the culture with RA and BMP2 from c3 onwards led to a down-regulation of BVSC at c7 and resulted in a significant reduction of BVSC at c9 (Figure 2A). Reciprocally, under this condition, VR began to be activated by c7 and a majority (~70%) of SC (+) cells at c9 exhibited VR (Figure 2A). IF analyses revealed that PGCLCs cultured with RA and BMP2 began to express STRA8, an essential factor for the entry into meiotic prophase (Anderson et al., 2008; Baltus et al., 2006), as early as c5 [~40.7%/SC (+) cells] and at c7, the vast majority (~91.7%) of SC (+) cells showed STRA8 and some of them (~27.1%) became positive for SCP3 (Figure 2B, C). Remarkably, at c9, more than 90% of SC (+) cells expressed SCP3 with its localization patterns indicative of the cells' entry into meiotic prophase, and the expression of STRA8 began to wane (Figure 2B, C). Interestingly, we noted that SCP3 exhibited a tendency to be up-regulated in a synchronous fashion in all the SC (+) cells comprising distinct colonies at a given time during the culture (Figure 2B, D). From c5 to c9, SC (+) cells exhibited clear positivity for DAZL (Figure 2B).

Meiotic entry is characterized by pre-meiotic DNA replication and arrest at the four-chromosome (4C) state (Baltus et al., 2006; Spiller and Bowles, 2015). In the presence of RA and BMP2, cultured BV/SC (+) cells exhibited a highly enhanced proliferation by c5 (~10-fold increase in number), appeared to cease proliferation by c7, and declined to approximately half their peak number by c9 (Figure 2E). The analysis of the cell-cycle state/DNA content revealed that at c7, a substantial fraction of BV/SC (+) cells were either replicating their DNAs (i.e., incorporating EdU) (~42.4%) or in the 4C state (~31%) (Figure 2F). At c9, remarkably, the vast majority (~86.8%) of BV/SC (+) cells were in the 4C state (Figure 2F). Combined with the expression dynamics of BVSCVR, STRA8 and SCP3, these findings are highly consistent with the idea that, in the presence of RA and BMP2, cultured PGCLCs take on the female fate and enter into meiotic prophase. Indeed, the spread analyses with γH2AX, a marker for double-strand breaks (DSBs) (Mahadevaiah et al., 2001), and the synaptonemal complex proteins SCP1 and SCP3 (Meuwissen et al., 1992; Yuan et al., 2000) revealed that the SC (+) cells progressed up to the pachytene stage (leptotene: ~50.4%; zygotene: ~47.8%; pachytene: ~1.8%) of the meiotic prophase (Figure 2G).

RA and its down-stream effector STRA8 have been proposed to play a central role in female sex determination, including meiotic entry (Baltus et al., 2006; Bowles et al., 2006; Dokshin et al., 2013; Koubova et al., 2006; Spiller and Bowles, 2015). On the other hand, under our condition, RA alone was insufficient to induce the female germ-cell fate: although the addition of RA to the PGCLC culture from c3 onwards activated DT/DAZL to a certain extent and progressively up-regulated STRA8 [~77.7% of BV/SC (+) cells expressed STRA8], it did not activate VR/DDX4 or SCP3 (Figure 1D, 2A, Figure S2A-D), and the BV/SC (+) cells with RA were found to be actively cycling even at c9 (Figure S2E). In contrast, unexpectedly, BMP2 alone was sufficient to induce VR, albeit

less effectively than RA and BMP2 (Figure 1E, Figure S2F-J), and the IF analyses revealed that BMP2 alone induced SCP3 (+) meiocytes at c9 (Figure S2J). Since our culture included 10% knockout serum replacement (KSR) and 2.5% fetal calf serum (FCS) (Ohta et al., 2017), we reasoned that the presence of RA activity in such components (Hore et al., 2016) might confer onto the PGCLCs the ability to take on the female fate in response to BMP signaling. In accordance with this idea, the culture of PGCLCs with BMP2 and an inhibitor for the RA receptor (RAR) (BMS493) (Koubova et al., 2006) abrogated the up-regulation of VR/DDX4 as well as the induction of SCP3 (Figure S2F-J). Similarly, the inhibition of BMP signaling by a specific inhibitor [LDN193189: an inhibitor for activin receptor-like kinase (Alk) 2/3] (Cuny et al., 2008) blocked the VR activation and meiotic entry elicited by RA and BMP2 in a dose-dependent fashion (Figure S2K, L). We conclude that RA and BMP signaling are necessary and, most likely, sufficient to induce PGCLCs into the female pathway and that RA or STRA8 alone is insufficient for such induction.

BMP and RA Commit PGCs to the Female Fate

We next examined the roles of RA and BMP signaling in female sex determination in PGCs. For this purpose, we isolated PGCs at E11.5 from *Stella-EGFP* (SG) transgenic embryos (Payer et al., 2006; Seki et al., 2007) by FACS and cultured them under our condition with or without RA, BMP2, or both for four days (RA and BMP2 were provided from c0) (Figure 3A). While neither the control culture nor the culture with RA alone induced SCP3 or significantly affected the SG and DDX4 expression, the culture with BMP2 alone induced expression and distinct localization of SCP3 and an apparent up-regulation of DDX4 in a significant fraction of cells (~22.9%), and such cells down-regulated SG (Figure 3B, C). The culture with RA and BMP2 substantially increased the induction of SCP3 (+)/DDX4 strongly (+)/SG-negative (−) cells (~65.6%) (Figure 3B, C).

We performed a culture of whole embryonic ovaries at E11.5 and examined the effects of inhibitors of RA or BMP signaling on the induction of female germ-cell fate (Figure 3D). While a great majority (~88.3%) of DDX4 (+) cells progressed into the meiotic prophase with characteristic SCP3 expression at c4 under the control condition, inhibition of RA signaling by a chemical inhibitor (BMS493) severely impaired such progression (Figure 3E, F), which is consistent with previous reports (Bowles et al., 2006; Koubova et al., 2006). Similarly, inhibition of BMP signaling by a chemical inhibitor (LDN193189) abrogated the progression into the female germ-cell fate (Figure 3E, F). We went on to examine the effect of BMP signaling inhibition under the in vivo condition by administering LDN193189 to pregnant females every 12 hrs after E11.5, which led to a severe impairment in the progression to the female-germ cell fate (Figure 3G, H). Collectively, these findings demonstrate that both PGCs and PGCLCs require RA and BMP signaling to acquire the female germ-cell fate.

Transcription Dynamics during Female Sex Determination of PGCLCs/PGCs

We went on to analyze the transcription dynamics during the female sex determination of PGCLCs/PGCs. We isolated total RNAs from PGCs [*Stella-EGFP* (+) cells at E9.5, E10.5, E11.5, E12.5 female, E12.5 male] (Kagiwada et al., 2013), fetal primary oocytes [*Stella-EGFP* (+) at E13.5 (Kagiwada et al., 2013), *DDX4-RFP* (+) at E14.5, E15.5], PSG [*Stella-EGFP* (+) at E13.5 (Kagiwada et al., 2013), *DDX4-RFP* (+) at E14.5, E15.5], PGCLCs cultured under the control condition (d4, c3, c5, c7, c9) (Ohta et al., 2017), PGCLCs cultured with RA from c3 onwards (c5 RA, c7 RA, c9 RA), and PGCLCs cultured with RA and BMP2 from c3 onwards (c5 RAB2, c7 RAB2, c9 RAB2), and analyzed their transcriptome by an RNA-sequencing (RNA-seq) methodology (Nakamura et al., 2015).

In agreement with our previous reports (Ohta et al., 2017), the unsupervised hierarchical clustering (UHC) revealed that PGCs that were sexually undifferentiated until E11.5 were clustered closely with d4 PGCLCs, and then with c3-c9 PGCLCs and PGCLCs at early time-points during stimulation with RA or RAB2 (c5 RA, c5 RAB2) (Figure 4A). Remarkably, fetal primary oocytes (E14.5, E15.5) and PSG (E14.5, E15.5) formed distinct clusters, respectively, and PGCLCs at c9 with RAB2 (c9 RAB2) were clustered tightly with fetal primary oocytes (Figure 4A). Germ cells that initiated sexual differentiation (male and female germ cells at E12.5, E13.5) and PGCLCs at c7 with RAB2 (c7 RAB2) and at c7/c9 with RA (c7/c9RA) formed distinct clusters between the cluster with sexually undifferentiated PGCs/PGCLCs and the cluster with fetal primary oocytes/c9 RAB2 cells/PSG (Figure 4A). In good agreement with these findings, principal component analyses (PCA) clustered sexually undifferentiated PGCs and d4/c3-c9 PGCLCs closely together, illuminated a progressive transition of female and male germ-cell properties along their development, and defined a parallel progression of PGCLCs cultured with RAB2 along the female pathway, with c9 RAB2 cells clustered closely with fetal primary oocytes at E14.5/E15.5 (Figure 2B). In contrast, PGCLCs cultured with RA appeared to gain the properties of fetal oocytes only partially (Figure 2B). Thus, cultured PGCLCs stimulated with RA and BMP2 recapitulate the female differentiation pathway to form fetal primary oocytes.

To facilitate understanding of the gene-expression dynamics associated with the sexual differentiation of germ cells/PGCLCs, we defined four classes of gene sets that characterize their developmental stages: early PGC genes [318 genes: $\log_2$ fold-change: E9.5 – male/female E14.5 > 2, $\log_2$(RPM+1) at E9.5 > 4], late germ-cell genes [254 genes: $\log_2$ fold-change: male/female E14.5 – E9.5 > 2, $\log_2$(RPM+1) at male/female E14.5 > 4], fetal oocyte genes [476 genes: $\log_2$ fold-change: female E14.5 – male E14.5 > 2, female E14.5 – E9.5 > 2, $\log_2$(RPM+1) at female E14.5 > 4], and PSG genes [323 genes: $\log_2$ fold-change: male E14.5 – female E14.5 > 2, male E14.5 – E9.5 > 2,

$\log_2$(RPM+1) at male E14.5 > 4] (Figure 4C) (Table S1). Early PGC genes were enriched with genes bearing gene ontology (GO) functional terms such as "negative regulation of cell differentiation" and "regulation of cell cycle" and included *Prdm1*, *Prdm14*, *Tfap2c*, *Nanog*, and *Sox2*; late germ-cell genes were enriched with genes for "sexual reproduction" and "gamete generation" and included *Dazl*, *Ddx4*, *Piwil2*, *Mael*, and *Mov10l1*; fetal oocyte genes were enriched with genes for "meiosis" and "female gamete generation" and included *Stra8*, *Rec8*, *Sycp3*, *Dmc1*, and *Sycp1*; and PSG genes were enriched with genes for "piRNA metabolic process" and "male gamete generation" and included *Nanos2*, *Dnmt3l*, *Tdrd9*, *Tdrd5*, and *Piwil1* (Figure 4C).

As shown in Figure 4C and D, PGCLCs cultured with RAB2 progressively acquired late germ-cell and fetal oocyte genes, while down-regulating early PGC genes. In contrast, PGCLCs cultured with RA manifested such progressions only partially (Figure 4C, D). For example, while, remarkably, c9 RAB2 cells up-regulated key genes for meiosis and oocyte development (both included in fetal oocyte genes) such as *Stra8*, *Rec8*, *Sycp3*, *Sycp1*, *Spo11*, *Dmc1*, *Hormad1* and *Prdm9* (for meiosis) and *Figla*, *Ybx2*, *Nobox*, and *Cpeb1* (for oocyte development) to levels similar to those in E14.5/E15.5 fetal oocytes, c9 RA cells failed to exhibit sufficient gain of a majority of genes for meiosis and oocyte development, although they up-regulated *Stra8* and *Rec8*, which have been known to respond to RA even in a heterologous cellular context (Mahony et al., 2011; Oulad-Abdelghani et al., 1996) (Figure 4E). We identified genes up-regulated in c9 RA cells compared to c9 RAB2 cells (323 genes: $\log_2$(RPM+1) > 4, $\log_2$ fold-change: c9 RA – c9 RAB2 > 1 and c9 RA – d4/c0 > 1: RA genes) (Figure S3A-D) (Table S1). Such genes were also up-regulated compared to fetal primary oocytes at E14.5/E15.5, were enriched with those for "cell adhesion", "vasculature development", and "embryonic organ development", and included *Hoxa5*, *Hesx1*, *Pax6*, *Lmx1b*, *Pitx2*, and *Dnmt3b* (Figure S3B, C). These findings demonstrate that BMP signaling is critical not only for robustly driving the female pathway, but also for repressing aberrant developmental pathways elicited by RA.

Role of STRA8 in Fetal Primary Oocyte Development

Stra8 has long been known as a key RA-responsive gene essential for meiotic entry (Anderson et al., 2008; Baltus et al., 2006; Dokshin et al., 2013; Soh et al., 2015). However, the role of STRA8 in the overall program of female sex determination in germ cells has not been adequately defined. We therefore went on to examine the effect of the loss of *Stra8* during the fetal primary oocyte differentiation from PGCLCs. We generated several lines of *Stra8* knockout BVSC ESCs (XY) using the CRISPR/Cas9 system (Ran et al., 2013a; Ran et al., 2013b) and confirmed the frame shift deletions within the targeted exon and loss of STRA8 expression in these lines (Figure S4A-C). We analyzed the properties of three independent lines [*Stra8* knockout (SK) 1, 2, 3], which exhibited essentially identical phenotypes (see below and data not shown). We therefore present

the results using the representative line, SK1. As shown in Figure 5A, while wild-type PGCLCs cultured with RAB2 exhibited down-regulation of BVSC from c7 and acquired a characteristic BVSC expression pattern at c9, SK1 cells continued to retain robust BVSC expression until c7 and exhibited a down-regulation of BVSC only at c9. Compared to wild-type cells, SK1 cells proliferated less effectively in response to RAB2 and yet continued to exhibit a cycling profile even at c9 (Figure 5B, C), indicating their failure to progress into the meiotic prophase.

We next determined the transcriptome of SK1 cells [SK1, 2 and 3 exhibited essentially identical transcriptomes (Figure S4D)]. PCA revealed that, compared to the wild-type RAB2 cells, SK1 RAB2 cells progressed along the female differentiation pathway in a protracted manner and, at c9, acquired a property similar to wild-type c7 cells, which was intermediate between fetal primary oocytes at E13.5 and E14.5 (Figure 5D). Compared to wild-type cells, SK1 cells exhibited a growing number of differentially expressed genes (DEGs) from c7 onwards (Figure 5E) (Table S2), and consistent with previous reports, the genes that were not fully up-regulated in c9 SK1 cells (178 genes: $\log_2$ fold-change: c9 wild-type RAB2 – c9 SK1 RAB2 > 2, $\log_2$(RPM+1) at c9 wild-type RAB2 > 4) were highly enriched with those for "meiosis" and "cell cycle process" and included *Prdm9*, *Sycp3*, *Spo11*, *Smc1b*, *Msh4*, *Msh5*, *Dmc1*, *Ccdc111*, and *Poln* (Figure 5F). However, it is of note that c9 SK1 cells up-regulated 32.1% of fetal oocyte genes (153/476 genes) in a relatively normal fashion ($\log_2$ fold-change: c9 wild-type RAB2 – c9 SK1 RAB2 < 1), including those associated with oocyte development, such as *Ybx2* and *Sohlh2* (Figure 5F-H). Interestingly, genes aberrantly up-regulated in c9 SK1 cells (138 genes: $\log_2$ fold-change: c9 SK1 RAB2 – c9 wild-type RAB2 > 2, $\log_2$(RPM+1) at c9 SK1 RAB2 > 4) were enriched with those for "embryonic organ development" and "chordate embryonic development", and were overlapped with the RA genes, i.e., those aberrantly up-regulated in c9 wild-type RA cells compared to c9 wild-type RAB2 cells (Figure 5G, Figure S3). On the other hand, c9 SK1 cells gained late germ-cell genes relatively normally [164/254 genes (64.6%): $\log_2$ fold-change: c9 wild-type RAB2 – c9 SK1 RAB2 < 1] (Figure 5F-H) (Table S2). These findings demonstrate that STRA8 is critical for ensuring sufficient expression levels of some of the genes involved in meiosis, as well as for repressing, in co-operation with an effector(s) of BMP signaling, aberrant developmental pathways elicited by RA.

Cellular Competence for Inducing the Female Fate in Response to RA and BMP

We next investigated a cellular context that leads to the female germ-cell fate in response to RA and BMP signaling, since BMP signaling specifies EpiLCs into PGCLCs, but it does not directly induces them into the female germ-cell pathway (Hayashi et al., 2011). For this purpose, we cultured d4/c0 and c7 PGCLCs with RA and BMP2 for two days, respectively, and evaluated their responses by examining their transcriptomes (Figure 6A, B). In comparison to the control culture, c7 PGCLCs provided with RA and BMP2

exhibited a substantial number of DEGs (log_2 fold-change > 2: up: 218 genes; down: 56 genes), with up-regulated genes being enriched with those for "meiosis", and progressed along the female pathway (Figure 6C, D) (Table S3). In contrast, d4/c0 PGCLCs provided with RA and BMP2 showed only a slight change in gene expression (log_2 fold-change > 2: up: 7 genes; down: 2 genes) and did not show a significant progression toward the female fate (Figure 6B, C) (Table S3). These findings demonstrate that PGCLCs acquire the competence to take on the female fate in response to RA and BMP during the expansion culture.

We have previously shown that, during the expansion culture, PGCLCs progressively erase their DNA methylome to acquire a state essentially identical to that of germ cells at E13.5, while maintaining their overall transcriptome and histone-modification states (Ohta et al., 2017). We here reasoned that the DNA methylation (5-methylcytosine: 5mC) states of key genes might underlie the acquisition of such competence during the PGCLC culture. To explore this possibility, we focused on an analysis of the relationship between the 5mC levels of promoters and the expression levels of genes categorized as those involved in "meiosis" [GO terms: Meiotic nuclear division GO: 0007126]. Among the 152 such genes analyzed (Table S3), 42 genes exhibited promoter demethylation of > 20% between d4/c0 and c7; these included *Stra8*, *Spo11*, *Sycp3*, *Dpep3*, *Dazl*, *Ddx4*, and *Piwil2*. On the other hand, 110 genes did not show significant promoter 5mC-level change (< 20%) during the culture; these consisted of genes involved in more general processes such as "DNA repair" and "response to DNA damage stimulus" and included *Mlh1*, *Brca2*, *Fanca*, *Cdc20* and *Plk1* (Figure 6E) (Table S3). In d4/c0 PGCLCs, the 42 genes showed high promoter 5mC levels and no/low expression, while the 110 genes were barely methylated and exhibited varying expression levels, the distribution of which was similar to that of all genes with low promoter 5mC levels (Figure 6E, F). In c7 PGCLCs, the 42 genes as well as nearly all other genes were demethylated, and, consistent with our previous observation (Ohta et al., 2017), some of the 42 genes such as *Dazl* and *Hormad1* were partially up-regulated, whereas the 110 genes remained un-methylated and retained an expression-level distribution similar to that in d4/c0 PGCLCs (Figure 6E). Remarkably, we found that in response to RA and BMP2 at c7, the 42 genes exhibited specific and robust activation, whereas the 110 genes showed only modest up-regulation (Figure 6E, F). Collectively, these findings support the notion that progressive promoter DNA demethylation of relevant genes during PGCLC expansion induces a basal activation or a permissive state for activation of such genes, which in turn acquire fully activated states in response to RA and BMP signaling to create the female germ-cell fate.

To validate the relevance of this notion to germ-cell development in vivo, we examined the relationship of expression differences of the 152 genes between E9.5 and E11.5 PGCs with those between d4/c0 and c7 PGCLCs, and then those between E11.5 PGCs and

E13.5 fetal primary oocytes with those between c7 PGCLCs and c7 PGCLCs stimulated by BMP2 and RA for two days. As shown in Figure 6G, the expression differences (up-regulation) of the 42 genes between successive stages of germ-cell and PGCLC development were highly correlated. In good agreement with this finding, PCA using the 152 genes clustered d4/c0 PGCLCs closely with E9.5 PGCs, c7 PGCLCs with E11.5 PGCs, and c7 PGCLCs cultured with RAB2 for 48 hrs with E13.5 female germ cells (Figure 6H). Based on these findings, we conclude that the PGCLC-based in vitro system precisely recapitulates the mechanism for the acquisition of the female germ-cell fate in vivo.

DISCUSSION

Using ESCs as a starting material, we have established an in vitro system that recapitulates germ-cell development from PGC specification up to fetal primary oocyte specification under a defined condition without the use of gonadal somatic cells. Based on this in vitro system as well as relevant in vivo analyses, we have demonstrated that a synergistic action of RA and BMP signaling confers the female germ-cell fate upon PGC(LCs) that have acquired an appropriate competence, at least partly as the result of genome-wide DNA demethylation (Figure 7). Thus, female germ-cell specification is an event that requires multiple signaling inputs and a proper epigenetic background in an integrated fashion (Figure 7).

The mechanism for sex determination of germ cells that occur in the middle of development has been difficult/laborious to analyze, due to the complexity of germ-soma interactions, and the redundancy/earlier requirements of relevant factors during development. For example, RA is present throughout the body and acts through three receptors with similar function, RARα, β and γ (Rhinn and Dolle, 2012); BMP signaling is essential for PGC specification (Lawson et al., 1999; Ying and Zhao, 2001); *Bmp2* is required for amnion/chorion and cardiac development and *Bmp2* knockout embryos die by E11.5 prior to sex determination (Zhang and Bradley, 1996); and both *Bmp2* and *Bmp5* are expressed in pre-granulosa cells (Figure S1F) (Jameson et al., 2012). Our system overcomes such difficulties and allows analyses for female sex determination of germ cells both in a reductive and a constructive fashion. Our data also demonstrate unambiguously that both XY and XX germ cells enter into the female pathway in a similar manner.

Classical observations that ectopic germ cells take on the female fate have led to a proposition that the female fate is a default pathway in germ cell development (McLaren and Southee, 1997; Zamboni and Upadhyay, 1983). Identification of RA as a critical inducer of the female germ-cell fate has revised this concept, and at the same time, has provided a rationale for the classical observations, since RA is not only present in embryonic ovaries but also broadly distributed throughout the body, yet, importantly, is actively degraded by CYP26B1 in nascent Sertoli cells in embryonic testes (Bowles et al., 2006; Koubova et al., 2006). However, we found that RA and its key downstream effector, STRA8, are not sufficient to induce the female fate in competent PGC(LC)s (Figure S2A-E), and that the combined action of RA and BMP signaling robustly induces competent PGC(LC)s into primary oocytes (Figure 2-4). In good agreement with this finding, the pre-granulosa cells that are likely instructive in specifying the female germ-cell fate have been shown to express high levels of *Bmp2* and *Bmp5* (Figure S1F) (Jameson et al., 2012)—particularly *Bmp2* in response to *Wnt4*, a key feminizing signal (Yao et al., 2004)—and a recent report demonstrated a critical function of *Smad4*, a transducer of BMP/TGFβ signaling, in the female sex determination of germ cells (Wu et

al., 2016). Moreover, the fact that all the BMP ligands that activate BMP receptor type II (BMPRII)-ALK3 signaling, including BMP2, BMP4, BMP5, and BMP7, are essentially capable of inducing the female fate (Figure S1G, H) would also explain a tendency for the ectopic germ cells to adopt the female fate (McLaren and Southee, 1997; Zamboni and Upadhyay, 1983).

The mechanism by which RA and BMP signaling elicit the female germ-cell program and drive the entry into meiosis remains unknown. The provision of RA signaling alone in PGCLCs resulted in full activation of STRA8, yet only partially up-regulated both late germ-cell genes and fetal oocyte genes, failed to repress early PGC genes, and ectopically up-regulated somatic genes (RA genes) such as those involved in "vasculature development" and "embryonic organ development", and consequently, the PGCLCs failed to initiate pre-meiotic DNA replication (Figure S2, S3). On the other hand, in the presence of RA and BMP signaling, *Stra8*-knockout PGCLCs acquired late germ-cell genes in a relatively normal manner, but failed to gain fetal oocyte genes (in particular, genes for meiosis) and to repress early PGC genes properly, and, interestingly, failed to repress RA-induced ectopic somatic program, which also resulted in a failure of PGCLCs to undergo pre-meiotic DNA replication (Figure 5). These findings suggest the possibility that a key downstream effector(s) of BMP signaling may cooperate with STRA8 to fully activate fetal oocyte genes and to repress the RA-induced somatic program and early PGC genes. Identification of a key downstream effector(s) of BMP signaling and investigation of its mechanisms of action, including the relationship with STRA8, will be one of the critical challenges in order to clarify the mechanism for female germ-cell specification and the synchronized entry into pre-meiotic DNA replication (Figure 2B-D) (Lei and Spradling, 2016).

We have shown that c7, but not d4/c0, PGCLCs were capable of immediately responding to RA and BMP signaling to up-regulate genes involved in "meiosis", and this difference in competence can be explained by the promoter demethylation of relevant genes during the expansion culture (Figure 6) (Ohta et al., 2017). This would also explain why early PGCs, which are specified by BMP signaling, are not directly induced into the meiotic program. In further support of this notion, we found that in the male pathway, KIT (+) spermatogonia at postnatal day 7 (P7), which are an immediate precursor which undergoes meiosis in the first wave of spermatogenesis, exhibited low/no 5mC levels in the promoters of the relevant 42 genes, despite the fact that they re-acquired high global 5mC levels during their development (Figure S5A) (Ishikura et al., 2016; Kubo et al., 2015). Interestingly, we found that these genes exhibited significant demethylation during the transition from KIT (−) spermatogonia at P7 (Figure S5A) (Kubo et al., 2015). Thus, the epigenetic requirements for meiotic entry appear to be in common, at least in part, between male and female germ cells.

During the 9-day culture period with the provision of RA and BMP from c3 onward, d4/c0 PGCLCs progressed up to the pachytene stage (~1.8%). We found that the addition of RA as early as c0 followed by the combined provision of BMP2 from c3 onward resulted in an enhanced maturation of PGCLCs as primary oocytes both at the cytological (leptotene: ~34.9%; zygotene: ~53.4%; pachytene: ~11.6%) and the transcriptome levels (Figure S5B, C), suggesting that it might be possible to extend the maturation of primary oocytes even further without the use of gonadal somatic cells under an appropriate condition, a possibility that warrants future investigation. The in vitro system that we have established recapitulates key processes of germ cell development, e.g., PGC specification, PGC propagation, epigenetic reprogramming and female sex determination, under a defined condition, and should serve as a critical foundation to explore the mechanisms underpinning such salient processes. Moreover, our strategy could be applied to exploration of the mechanism for male sex determination as well as to the development of a culture method for the maturation and sex determination of PGCLCs of other key species, including humans.

AUTHOR CONTRIBUTIONS

H.M. conducted all the experiments and analyzed the data. H.O. contributed to the PGCLC propagation, S.O. and F.N. contributed to the analyses of meiotic cells, and K.H. contributed to the PGCLC induction. Y.Y. contributed to the analysis of the WGBS data, and Y.Y., T.N., and T.Y. contributed to the RNA-seq. M.S. conceived the project, and H.M. and M.S. designed the experiments and wrote the manuscript.

ACKNOWLEDGMENTS

We thank K. Abe and T. Noce for providing us with the *mVH-RFP* mice. We are grateful to the members of the Saitou Laboratory for their discussion of this study. We thank Y. Nagai, R. Kabata, N. Konishi, Y. Sakaguchi, and M. Kawasaki of the Saitou Laboratory, and T. Sato and M. Kabata of the Yamamoto Laboratory for their technical assistance. This work was supported in part by JST-ERATO to M.S.

EXPERIMENTAL PROCEDURES

Animals

All animal experiments were performed under the ethical guidelines of Kyoto University. The BVSC (Acc. No. BV, CDB0460T; SC CDB0465T: http://www.cdb.riken.jp/arg/TG%20mutant%20mice%20list.html), *Stella-EGFP* (SG), and *mVH-RFP* (VR) transgenic mice were established as reported previously (Imamura et al., 2010; Ohinata et al., 2008; Payer et al., 2006; Seki et al., 2007) and were maintained on a largely C57BL/6 background. The *Dazl-tdTomato* (DT) mice were generated by injecting the BVSCDT ESCs (XY) into the blastocysts (ICR) followed by their transfer to foster mothers. The ICR mice were purchased from SLC (Shizuoka, Japan). Noon of the day when a copulation plug was identified was designated as embryonic day (E) 0.5.

For administering LDN-193189 into pregnant females (ICR), LDN-193189 (sml0559; Sigma-Aldrich) was dissolved in sterile water and 2.5 mg of the LDN-193189 per kg body weight was injected intra-peritoneally every 12 hrs from E11.5 to E14.

ESC Culture/Derivation and PGCLC Induction/Culture

H18 BVSC ESCs (XX) (Hayashi et al., 2012), R8 BVSC ESCs (XY) (Hayashi et al., 2011), L9 BVSCVR ESCs (XX), L5 BVSCVR ESCs (XY), BVSCDT ESCs (XY; a subline of R8), BDF1-2-1 BVSC ESCs (XY) (Ohta et al., 2017), and *Stra8*-knockout BVSC ESCs (SK1, 2, 3; XY; sublines of BDF1-2-1) were used for this study. L5 and L9 BVSCVR ESCs were established from blastocysts obtained through matings of the VR females (Imamura et al., 2010) with the BVSC males (Ohinata et al., 2008), according to a procedure described previously, and were adapted to a feeder-free condition (Hayashi et al., 2011). The procedures for the establishment of BVSCDT and *Stra8*-knockout ESCs are described below in the "**Establishment of the BVSCDT ESCs"** and **"Establishment of *Stra8*-knockout ESCs"** sections, respectively.

The ESC culture and PGCLC induction were performed as described previously (Hayashi et al., 2011; Hayashi and Saitou, 2013) with a few modifications. ESCs were maintained under a 2i+LIF condition on a dish coated with poly-L-ornithine (0.01%; Sigma) and Laminin (300 ng/ml; BD Biosciences) or on mouse embryonic fibroblasts (MEF). EpiLCs were induced by plating 1.0×10^5 ESCs on wells of a 12-well plate coated with human plasma fibronectin (16.7 ug/ml; Millipore) in N2B27 medium containing activin A (20 ng/ml; Peprotech), bFGF (12 ng/ml; Life Technology) and KSR (1%; Thermo Fisher). 42-46 hrs after the EpiLC induction, PGCLCs were induced under a floating condition by plating 2.0×10^3 EpiLCs in wells of a low-cell-binding 96-well Lipidure-coat plate (Thermo Fisher) in 200 μl of GK15 medium with BMP4 (500 ng/ml; R&D Systems), LIF (1000 u/ml; Merck Millipore), SCF (100 ng/ml; R&D Systems), and EGF (50 ng/ml; R&D Systems). The GK15 medium was composed of GMEM (Thermo Fisher) with 15% KSR, 0.1 mM NEAA, 1 mM sodium pyruvate, 0.1 mM

2-mercaptoethanol, 100 U/ml penicillin, 0.1 mg/ml streptomycin and 2 mM L-glutamine.

The PGC/PGCLC culture was performed as described previously (Ohta et al., 2017). Briefly, d4 PGCLC aggregates were collected, washed with PBS, and dissociated with TrypLE Express (Thermo Fisher). They were then washed with DMEM+0.1%BSA (Gibco) and filtered by a cell strainer (BD Bioscience) to remove large clumps of cells. Next, the samples were centrifuged, resuspended in 0.1% BSA-PBS and sorted by FACS (Aria lll; BD Bioscience). The BV (+) cells were plated onto mitomycin C (MMC)-treated m220 feeder cells in the PGC/PGCLC-expansion medium. The PGC/PGCLC-expansion medium was composed of GMEM with 10% KSR, 2.5% FBS, 0.1 mM NEAA, 1 mM sodium pyruvate, 2 mM L-glutamine, 0.1 mM 2-mercaptoethanol, 100 U/ml penicillin, 0.1 mg/ml streptomycin, 10 μM Forskolin and 10 μM Rolipram. The entire medium was changed every 2 days from c3. The cytokines/chemicals for the induction of the female fate were provided from c3 to the end of the culture. The concentrations of RA and BMP used were 100 nM and 300 ng/mL, respectively, unless otherwise specified. Bright field and fluorescence images were captured using an IX73 inverted microscope (Olympus).

Establishment of the BVSCDT ESCs

To construct the donor vector for the generation of *Dazl-tdTomato* (DT) knockin ESCs, the homology arms of *Dazl* (the fragments from 1,048 bp upstream and to 1,247 bp downstream of the stop codon, respectively) were amplified from the genomic DNA of R8 BVSC ESCs by PCR **(Primers)**, and were sub-cloned into the pCR2.1 vector (TOPO TA Cloning; Life Technologies). The *p2A-tdTomato* fragment with the *Pgk-Puro* cassette flanked by the *LoxP* sites was amplified by PCR from the vector reported previously (Sasaki et al., 2015), and inserted in-frame at the 3-prime end of the *Dazl* coding sequence of the sub-cloned vector containing the homology arms, using a GeneArt Seamless Cloning & Assembly Kit (Life Technologies). The stop codon was removed for the expression of the in-frame fusion protein.

The TALEN constructs targeting the sequences adjacent to the stop codon of *Dazl* were generated using a GoldenGate TALEN and TAL Effector kit (Addgene #1000000016) as described previously (Sakuma et al., 2013; Sasaki et al., 2015). The activities of the TALENs were evaluated by a single-strand annealing (SSA) assay.

The donor vector (5 μg) and the TALEN plasmids (10 μg each) were introduced into the R8 BVSC ESCs by electroporation using a NEPA21 type II electroporator (Nepagene). Single colonies were picked up after puromycin selection, and random or targeted integrations were evaluated by PCR **(Primers)**, followed by verification by Southern blot analyses. The line with the correct targeting was transfected with a plasmid expressing Cre recombinase to remove the *Pgk-Puro* cassette.

Establishment of *Stra8*-knockout ESCs

The vector expressing the Cas9 nickase (Addgene #42335) fused in frame with a reporter gene GSG-p2A-mCherry was created (the mCherry used contained a silent mutation, 432G>A). Two pairs of oligonucleotides **(Primers)** for targeting exon 6 of *Stra8* were annealed, phosphorylated, and ligated separately to the above-mentioned vector digested by Bbsl (NEB), according to the reported protocols (Ran et al., 2013a; Ran et al., 2013b). The activities of the nickases were evaluated by the SSA assay. The pair of nickase plasmids (200 ng each) was introduced into the BDF1-2-1 BVSC ESCs by electroporation using the NEPA21 type II electroporator. The ESCs were dissociated two days after the transfection, and single cells expressing high levels of mCherry, which are expected to also express high levels of the Cas9 nickase, were sorted by FACS and seeded onto MEFs in single wells of 96-well plates so that each well contained a single clone. The clones were cultured and expanded, and the disruption of the *Stra8* loci in the clones was assessed by Sanger sequencing of the PCR products of the relevant region **(Primers)**. The *Stra8* knockout was confirmed by Western blot and IF analyses.

***Ex Vivo* Culture of PGCs or Embryonic Gonads**

For the PGC culture, embryonic gonads (not sex-typed) of the SG mice at E11.5 were dissected and dissociated. SG (+) PGCs were sorted by FACS, plated onto m220 feeder cells, and cultured in the PGC/PGCLC-expansion medium. The reagents for the induction of the female fate were provided from c0.

For the culture of the embryonic gonads, embryonic ovaries with mesonephroi at E11.5 [sex-typed by PCR **(Primers)**] were dissected out and cultured under a gas-liquid interface condition on the culture inserts (353095; BD Falcon). The medium used was DMEM with 10% FBS, 100 U/ml penicillin, 0.1 mg/ml streptomycin and 2 mM L-glutamine. Chemical inhibitors were provided with the medium from c0.

Fluorescence-activated Cell Sorting (FACS), Cell-cycle Analysis, and Cell Counting

The preparation of d4/c0 PGCLCs for FACS was described in "**ESC Culture/Derivation and PGCLC Induction/Culture"**. As for germ cells in vivo, embryonic gonads of BVSC, VR or SG mice were dissected and processed for FACS according to the procedure described for d4/c0 PGCLCs. Cultured PGCLCs were also prepared in a similar manner, except that after dissociation, they were washed with 0.1%BSA-DMEM containing 100 μg/ml DNasel (Sigma-Aldrich) to digest DNA lysed out from dead cells to prevent the formation of cell/debris clumps. The fluorescence activities of BV/SG, SC or DT/VR were detected in the FITC, Horizon V500 or PE-Texas Red channel, respectively. The FACS data were analyzed using the FlowJo or FACS Diva software packages.

The cell-cycle analysis was performed using a Click-iT EdU Flow Cytometry Assay Kit (C10424; Thermo Fischer Scientific) according to the manufacturer's instructions. Cultured PGCLCs were treated with 10 μg/ml of EdU for 30 min to 2 hrs and were analyzed by FACS.

Cultured PGCLCs were stained with a chicken anti-GFP antibody followed by an Alexa Fluor 633 goat anti-chicken antibody, and were analyzed using a Cellavista instrument (SynenTec) (Ohta et al., 2017).

Cytokines/Chemicals

The cytokines/chemicals used to screen for activities involved in the induction of the female fate were as follows (Figure 1): 100 nM all-trans retinoic acid, 500 ng/ml WNT4 (R&D Systems), 500 ng/ml RSPO1 (R&D Systems), 100 ng/ml FGF9 (R&D Systems), 500 ng/ml PgD2 (Cayman), 25 ng/ml activin A, 100 ng/ml NODAL (R&D Systems), 500 ng/ml SDF1 (R&D Systems), 50 ng/ml bFGF, 500 ng/ml BMP2 (R&D Systems), 500 ng/ml BMP4 (R&D Systems), 500 ng/ml BMP5 (R&D Systems), 500 ng/ml BMP7 (R&D Systems), 250 ng/ml WNT5a (R&D Systems), and 1000 U/ml LIF. In the signal inhibition experiments, LDN193189 (#04-0074; Stemgent) and BMS493 (B6688; Sigma-Aldrich), which were dissolved in DMSO, were used as an ALK2/3 inhibitor and an RAR inhibitor, respectively.

Immunofluorescence (IF) Analysis

Immunofluorescence (IF) analysis was performed as described previously (Hayashi et al., 2012). The following primary antibodies were used: chicken anti-GFP (ab13970; abcam), rabbit anti-DDX4 (ab13840; abcam), mouse anti-DDX4 (ab27591; abcam), rabbit anti-DAZL (ab34129; abcam), goat anti-DAZL (sc-27333; SantaCruz), rabbit anti-STRA8 (ab49602; abcam) and mouse anti-SYCP3 (ab97672; abcam). The following secondary antibodies were used: Alexa Fluor 488 goat anti-mouse or -chicken IgG; Alexa Fluor 568 goat anti-rabbit IgG and Alexa Fluor 633 goat anti-mouse, -chicken IgG; Alexa Fluor 488 donkey anti-mouse IgG; Alexa Fluor 568 donkey anti-rabbit IgG and Alexa Fluor 633 donkey anti-goat IgG. IF images were captured using a confocal microscope [FV1000 (Olympus) or LSM 780 (Zeiss)].

Spread Analysis of the Meiotic Chromosomes in Fetal Oocyte-like Cells

Spread preparations and IF analyses were performed as described previously with minor modifications (Yamashiro et al., 2016). c9 RAB2 cells were sorted by FACS and the sorted cells were washed with PBS and treated in a hypotonic-extraction solution at 25°C for 1 hr. The primary antibodies used were as follows: goat anti-SCP3 (1:250; sc-20845; Santa Cruz), mouse anti-γH2AX (1:1000; 05-636; Millipore), and rabbit anti-SCP1 antibody (1:250; NB300-229; Novus). The secondary antibodies used were as follows: Alexa Fluor 488 donkey anti-goat IgG (A11055; Thermo Fisher), Alexa Fluor 568

donkey anti-rabbit IgG (A10042; Thermo Fisher), and Alexa 647 donkey anti-mouse IgG (A31571; Thermo Fisher). We counted SYCP3 (+) cells and the definition of the meiosis stages was as follows: Leptotene: γH2AX (+) and SYCP1 (−); Zygotene: γH2AX(+) and SYCP1 (+); Pachytene: SYCP1(++) in at least 80% of the chromosomes.

Southern Blot Analysis

Southern blot analysis was performed as described previously (Nakaki et al., 2013). Briefly, 10 μg of genomic DNA was digested with the restriction enzymes and the resulting DNA fragments were electrophoresed in 0.9% agarose gel, transferred to the Hybond N+ membrane (RPN303B; GE Healthcare), and baked for the crosslink. The DIG-labeled probes for *tdTomato*, and the 5 and 3 prime sides of the relevant region of *Dazl* were generated by PCR (PCR DIG Labeling Mix; Sigma-Aldrich) **(Primers)**. Images were captured using an LAS4000 (Fujifilm).

Western Blot Analysis

For the Western blot analysis, 5×10^4 cells were lysed with the SDS sample buffer [62.5 mM Tris-HCl (pH 6.8), 2% SDS, 10% glycerol, 0.025% bromophenol blue and 0.14 M –mercaptoethanol] at 90°C for 5 min, and the extracted proteins were separated on SuperSep Ace 10-20% gels (Wako), blotted onto the iBlot2 PVDF transfer membrane (Thermo Fisher) by an iBlot2 dry blotting system (Thermo Fisher), and incubated with primary antibodies: rabbit anti-STRA8 IgG (ab49405; abcam) or mouse anti-α-TUBULIN (T9026; Sigma-Aldrich). The primary antibodies were detected with the goat anti-rabbit or sheep anti-mouse IgG conjugated with HRP (A0545, M8642; Sigma-Aldrich) followed by detection using Chemi-Lumi One Super (Nacalai). The chemiluminescence images were captured with a Fusion Solo (M&S Instruments).

Transcriptome Analysis

E14.5 and E15.5 male and female germ cells were collected as VR (+) cells and cultured PGCLCs as SC (+) cells by FACS, and total RNAs of the samples were extracted and purified using an RNeasy Micro Kit (74004; QIAGEN) according to the manufacturer's instructions. The cDNAs synthesis, library construction and analysis by Nextseq500 (Illumina) from 1 ng of total RNAs from each sample were performed according to the methods described previously (Ishikura et al., 2016; Nakamura et al., 2015). The cDNAs of germ cells from E9.5 to E13.5 prepared in previous studies (Kagiwada et al., 2013; Ohta et al., 2017) were also analyzed by the Nextseq500 sequencer system.

All the read data were converted into expression levels as described previously (Nakamura et al., 2015). Briefly, all reads were treated with cutadapt-1.3 (Martin, 2011) to remove the V1 and V3 adaptor sequences and the poly-A sequences. The resulting reads of 30-bp or longer were mapped onto the mm10 genome using TopHat1.4.1/Bowtie1.0.1 with the "-no-coverage-search" option (Kim et al., 2013).

Mapped reads were then converted to the expression level (RPM) using cufflinks-2.2.0 with the "-compatible-hits-norm", "-no-length-correction", "-max-mle-iterations 50000" and "library-type fr-secondstrand" options, and mm1-reference gene annotation with up to 10-kb extension at the 3'-ends. The entire gene set analyzed was the same as that in our previous study (Ishikura et al., 2016).

Transcriptome analysis was performed using the R software package, version 3.2.1 with the gplots package and Microsoft Excel. First, the expression raw data were converted into $\log_2$(RPM+1) values, and genes with expression values > 2 in at least one sample were defined as expressed, unless otherwise specified. Data processing (e.g., identification of DEGs) was performed by using average values of biological replicates, except for the construction of the heat maps, clustering, and PCA. To create heat maps, the gplots package (heatmap.2) was used. Gene ontology (GO) analysis was performed by using the DAVID 6.7 website (https://david.ncifcrf.gov) (Huang da et al., 2009).

Analysis of the DNA Methylation of Promoters

Whole-genome bisulfite sequencing (WGBS) data of ESCs, EpiLCs and PGCLCs were obtained from our previous studies (Ohta et al., 2017; Shirane et al., 2016), and those of KIT (−) and KIT (+) spermatogonia were obtained from a previous study (Kubo et al., 2015). We here defined promoters as regions between 900-bp upstream and 400-bp downstream of the transcription start sites (TSSs), and all the percent 5-methylcytosine values (% 5mC) were calculated from the average of CpGs, in which the read depth was between 4 and 200, as previously described (Ishikura et al., 2016).

Primers

Sex typing

Gene	Forward primer	Reverse primer
Ubal	TGGATGGTGTGGCCAATGCYCT	CCACCTGCACGTTGCCCTTKGTGCCCAG

Vector construction for *Dazl-tdTomato*

Dazl forward	AGAATCTGGTCCACAGGAAAAGGGCCTGAT
Dazl reverse	AGGCTTAGCCCCTGAGCTGCTTGTTAACTG
Genotype forward	AATAGACCCTAACCAGTTGGTGCAT
Genotype reverse	AAGAGTAAGTGGAATCCATGTTTGAAGGA
Random Integration forward	CCGGATGAATGTCAGCTACTGGGCTATCTG
Random Integration reverse	TTCGGGGCGAAAACTCTCAAGGATCTTACC

Stra8-knockout

Nickase1 forward	CACCgGAGATGGCGGCAGAGACAAT
Nickase1 reverse	AAACATTGTCTCTGCCGCCATCTCc
Nickase2 forward	CACCgCCTGTGGCAGACTCTCTCTG
Nickase2 reverse	AAACCAGAGAGAGTCTGCCACAGGc

Sequence forward	TAAGGCCAGGGGAAGGCAGAC
Sequence reverse	CGAAGGGCCATCTCACAGGGTC

Southern blot analysis

5' probe forward	GGAGGCAAAGACAGGATCCTAAGCAAACTA
5' probe reverse	TCCCTAGTGCTCTATAAAATTGAGGTAATT
tomato probe forward	CCGCCGACATCCCCGATTAC
tomato probe reverse	GCAGTTGCACGGGCTTCTTG
3' probe forward	ACCAGAAAACTAAGAAGTGTCCTGAA
3' probe reverse	AGACAGGACAGTAAGTCAGTGATGCT

Antibodies

Antibody	**Supplier**	**Catalogue #**	**Application**
Chicken anti-GFP	Abcam	Ab13970	IF
Rabbit anti-DDX4	Abcam	Ab13840	IF
Mouse anti-DDX4	Abcam	Ab27591	IF
Goat anti-DAZL	SantaCruz	Sc-27333	IF
Rabbit anti-STRA8	Abcam	Ab49602	IF
Mouse anti-SYCP3	Abcam	Ab97672	IF
Goat anti-SCP3	SantaCruz	Sc-20845	IF (Spread)
Mouse anti-γH2AX	Millipore	05-636	IF (Spread)
Rabbit anti-SCP1	Novus	NB300-299	IF (Spread)
Rabbit anti-STRA8	Abcam	Ab49405	WB
Mouse anti-α-TUBULIN	Sigma-Aldrich	T9026	WB

ACCESSION NUMBERS

The accession numbers of the data used in this study are as follows: the RNA-seq data of E10.5 and E11.5 PGCs and E13.5 female germ cells in Figure 4 (GEO: GSE74094) (Yamashiro et al., 2016), the RNA-seq data of E9.5 PGCs and E12.5 female germ cells in Figure 4 (GEO: GSE87644) (Ohta et al., 2017), the RNA-seq data of d4 PGCLCs in Figure 4 (GEO: GSE67259) (Sasaki et al., 2015), the microarray data of E11.5, E12.5, and E13.5 male and female supporting cells (GEO: GSE27715) (Jameson et al., 2012), the WGBS data of ESCs, EpiLCs, and d4 PGCLCs (DDBJ: DRA003471) (Shirane et al., 2016), the WGBS data of c7 PGCLCs (DDBJ: DDBJ: DRA005166) (Ohta et al., 2017), and the WGBS data of P7 KIT^{-} SG and KIT^{+} SG (DDBJ: DRA002477) (Kubo et al., 2015).

The RNA-seq data of E9.5, E10.5, and E11.5 PGCs, E12.5, E13.5, E14.5, and E15.5 male and female germ cells, and cultured PGCLCs under the described conditions are in the process of being registered.

REFERENCES

Anderson, E.L., Baltus, A.E., Roepers-Gajadien, H.L., Hassold, T.J., de Rooij, D.G., van Pelt, A.M., and Page, D.C. (2008). Stra8 and its inducer, retinoic acid, regulate meiotic initiation in both spermatogenesis and oogenesis in mice. Proc Natl Acad Sci U S A *105*, 14976-14980.

Baltus, A.E., Menke, D.B., Hu, Y.C., Goodheart, M.L., Carpenter, A.E., de Rooij, D.G., and Page, D.C. (2006). In germ cells of mouse embryonic ovaries, the decision to enter meiosis precedes premeiotic DNA replication. Nat Genet *38*, 1430-1434.

Baudat, F., Imai, Y., and de Massy, B. (2013). Meiotic recombination in mammals: localization and regulation. Nat Rev Genet *14*, 794-806.

Bowles, J., Knight, D., Smith, C., Wilhelm, D., Richman, J., Mamiya, S., Yashiro, K., Chawengsaksophak, K., Wilson, M.J., Rossant, J*., et al.* (2006). Retinoid signaling determines germ cell fate in mice. Science *312*, 596-600.

Cooke, H.J., Lee, M., Kerr, S., and Ruggiu, M. (1996). A murine homologue of the human DAZ gene is autosomal and expressed only in male and female gonads. Hum Mol Genet *5*, 513-516.

Cuny, G.D., Yu, P.B., Laha, J.K., Xing, X., Liu, J.F., Lai, C.S., Deng, D.Y., Sachidanandan, C., Bloch, K.D., and Peterson, R.T. (2008). Structure-activity relationship study of bone morphogenetic protein (BMP) signaling inhibitors. Bioorg Med Chem Lett *18*, 4388-4392.

Dokshin, G.A., Baltus, A.E., Eppig, J.J., and Page, D.C. (2013). Oocyte differentiation is genetically dissociable from meiosis in mice. Nat Genet *45*, 877-883.

Evans, E.P., Ford, C.E., and Lyon, M.F. (1977). Direct evidence of the capacity of the XY germ cell in the mouse to become an oocyte. Nature *267*, 430-431.

Fujiwara, Y., Komiya, T., Kawabata, H., Sato, M., Fujimoto, H., Furusawa, M., and Noce, T. (1994). Isolation of a DEAD-family protein gene that encodes a murine homolog of Drosophila vasa and its specific expression in germ cell lineage. Proc Natl Acad Sci U S A *91*, 12258-12262.

Gill, M.E., Hu, Y.C., Lin, Y., and Page, D.C. (2011). Licensing of gametogenesis, dependent on RNA binding protein DAZL, as a gateway to sexual differentiation of fetal germ cells. Proc Natl Acad Sci U S A *108*, 7443-7448.

Handel, M.A., and Schimenti, J.C. (2010). Genetics of mammalian meiosis: regulation, dynamics and impact on fertility. Nat Rev Genet *11*, 124-136.

Hayashi, K., Ogushi, S., Kurimoto, K., Shimamoto, S., Ohta, H., and Saitou, M. (2012). Offspring from oocytes derived from in vitro primordial germ cell-like cells in mice. Science *338*, 971-975.

Hayashi, K., Ohta, H., Kurimoto, K., Aramaki, S., and Saitou, M. (2011). Reconstitution of the mouse germ cell specification pathway in culture by pluripotent stem cells. Cell *146*, 519-532.

Hayashi, K., and Saitou, M. (2013). Generation of eggs from mouse embryonic stem cells and induced pluripotent stem cells. Nature protocols *8*, 1513-1524.

Hikabe, O., Hamazaki, N., Nagamatsu, G., Obata, Y., Hirao, Y., Hamada, N., Shimamoto, S., Imamura, T., Nakashima, K., Saitou, M.*, et al.* (2016). Reconstitution in vitro of the entire cycle of the mouse female germ line. Nature *539*, 299-303.
Hore, T.A., von Meyenn, F., Ravichandran, M., Bachman, M., Ficz, G., Oxley, D., Santos, F., Balasubramanian, S., Jurkowski, T.P., and Reik, W. (2016). Retinol and ascorbate drive erasure of epigenetic memory and enhance reprogramming to naive pluripotency by complementary mechanisms. Proc Natl Acad Sci U S A *113*, 12202-12207.
Huang da, W., Sherman, B.T., and Lempicki, R.A. (2009). Systematic and integrative analysis of large gene lists using DAVID bioinformatics resources. Nature protocols *4*, 44-57.
Imamura, M., Aoi, T., Tokumasu, A., Mise, N., Abe, K., Yamanaka, S., and Noce, T. (2010). Induction of primordial germ cells from mouse induced pluripotent stem cells derived from adult hepatocytes. Mol Reprod Dev *77*, 802-811.
Ishikura, Y., Yabuta, Y., Ohta, H., Hayashi, K., Nakamura, T., Okamoto, I., Yamamoto, T., Kurimoto, K., Shirane, K., Sasaki, H.*, et al.* (2016). In Vitro Derivation and Propagation of Spermatogonial Stem Cell Activity from Mouse Pluripotent Stem Cells. Cell reports *17*, 2789-2804.
Jameson, S.A., Natarajan, A., Cool, J., DeFalco, T., Maatouk, D.M., Mork, L., Munger, S.C., and Capel, B. (2012). Temporal transcriptional profiling of somatic and germ cells reveals biased lineage priming of sexual fate in the fetal mouse gonad. PLoS Genet *8*, e1002575.
Kagiwada, S., Kurimoto, K., Hirota, T., Yamaji, M., and Saitou, M. (2013). Replication-coupled passive DNA demethylation for the erasure of genome imprints in mice. EMBO J *32*, 340-353.
Kim, D., Pertea, G., Trapnell, C., Pimentel, H., Kelley, R., and Salzberg, S.L. (2013). TopHat2: accurate alignment of transcriptomes in the presence of insertions, deletions and gene fusions. Genome Biol *14*, R36.
Koubova, J., Menke, D.B., Zhou, Q., Capel, B., Griswold, M.D., and Page, D.C. (2006). Retinoic acid regulates sex-specific timing of meiotic initiation in mice. Proc Natl Acad Sci U S A *103*, 2474-2479.
Kubo, N., Toh, H., Shirane, K., Shirakawa, T., Kobayashi, H., Sato, T., Sone, H., Sato, Y., Tomizawa, S., Tsurusaki, Y.*, et al.* (2015). DNA methylation and gene expression dynamics during spermatogonial stem cell differentiation in the early postnatal mouse testis. BMC Genomics *16*, 624.
Lawson, K.A., Dunn, N.R., Roelen, B.A., Zeinstra, L.M., Davis, A.M., Wright, C.V., Korving, J.P., and Hogan, B.L. (1999). Bmp4 is required for the generation of primordial germ cells in the mouse embryo. Genes Dev *13*, 424-436.
Lei, L., and Spradling, A.C. (2016). Mouse oocytes differentiate through organelle enrichment from sister cyst germ cells. Science *352*, 95-99.
Lin, Y., Gill, M.E., Koubova, J., and Page, D.C. (2008). Germ cell-intrinsic and -extrinsic

factors govern meiotic initiation in mouse embryos. Science *322*, 1685-1687.
Lin, Y.T., and Capel, B. (2015). Cell fate commitment during mammalian sex determination. Curr Opin Genet Dev *32*, 144-152.
Mahadevaiah, S.K., Turner, J.M., Baudat, F., Rogakou, E.P., de Boer, P., Blanco-Rodriguez, J., Jasin, M., Keeney, S., Bonner, W.M., and Burgoyne, P.S. (2001). Recombinational DNA double-strand breaks in mice precede synapsis. Nat Genet *27*, 271-276.
Mahony, S., Mazzoni, E.O., McCuine, S., Young, R.A., Wichterle, H., and Gifford, D.K. (2011). Ligand-dependent dynamics of retinoic acid receptor binding during early neurogenesis. Genome Biol *12*, R2.
Martin, M. (2011). Cutadapt removes adapter sequences from high-throughput sequencing reads. EMBnetjournal *17*, 10.
McLaren, A., and Southee, D. (1997). Entry of mouse embryonic germ cells into meiosis. Dev Biol *187*, 107-113.
Meuwissen, R.L., Offenberg, H.H., Dietrich, A.J., Riesewijk, A., van Iersel, M., and Heyting, C. (1992). A coiled-coil related protein specific for synapsed regions of meiotic prophase chromosomes. EMBO J *11*, 5091-5100.
Nakaki, F., Hayashi, K., Ohta, H., Kurimoto, K., Yabuta, Y., and Saitou, M. (2013). Induction of mouse germ-cell fate by transcription factors in vitro. Nature *501*, 222-226.
Nakamura, T., Yabuta, Y., Okamoto, I., Aramaki, S., Yokobayashi, S., Kurimoto, K., Sekiguchi, K., Nakagawa, M., Yamamoto, T., and Saitou, M. (2015). SC3-seq: a method for highly parallel and quantitative measurement of single-cell gene expression. Nucleic Acids Res *43*, e60.
Ohinata, Y., Ohta, H., Shigeta, M., Yamanaka, K., Wakayama, T., and Saitou, M. (2009). A signaling principle for the specification of the germ cell lineage in mice. Cell *137*, 571-584.
Ohinata, Y., Sano, M., Shigeta, M., Yamanaka, K., and Saitou, M. (2008). A comprehensive, non-invasive visualization of primordial germ cell development in mice by the Prdm1-mVenus and Dppa3-ECFP double transgenic reporter. Reproduction *136*, 503-514.
Ohta, H., Kurimoto, K., Okamoto, I., Nakamura, T., Yabuta, Y., Miyauchi, H., Yamamoto, T., Okuno, Y., Hagiwara, M., Shirane, K.*, et al.* (2017). Expansion of mouse primordial germ cell-like cells in culture reconstitutes an epigenetic blank slate. EMBO J *Under Revision*.
Oulad-Abdelghani, M., Bouillet, P., Decimo, D., Gansmuller, A., Heyberger, S., Dolle, P., Bronner, S., Lutz, Y., and Chambon, P. (1996). Characterization of a premeiotic germ cell-specific cytoplasmic protein encoded by Stra8, a novel retinoic acid-responsive gene. J Cell Biol *135*, 469-477.
Payer, B., Chuva de Sousa Lopes, S.M., Barton, S.C., Lee, C., Saitou, M., and Surani, M.A. (2006). Generation of stella-GFP transgenic mice: a novel tool to study germ cell development. Genesis *44*, 75-83.

Pepling, M.E., and Spradling, A.C. (1998). Female mouse germ cells form synchronously dividing cysts. Development *125*, 3323-3328.
Ran, F.A., Hsu, P.D., Lin, C.Y., Gootenberg, J.S., Konermann, S., Trevino, A.E., Scott, D.A., Inoue, A., Matoba, S., Zhang, Y.*, et al.* (2013a). Double nicking by RNA-guided CRISPR Cas9 for enhanced genome editing specificity. Cell *154*, 1380-1389.
Ran, F.A., Hsu, P.D., Wright, J., Agarwala, V., Scott, D.A., and Zhang, F. (2013b). Genome engineering using the CRISPR-Cas9 system. Nature protocols *8*, 2281-2308.
Rhinn, M., and Dolle, P. (2012). Retinoic acid signalling during development. Development *139*, 843-858.
Saitou, M., Barton, S.C., and Surani, M.A. (2002). A molecular programme for the specification of germ cell fate in mice. Nature *418*, 293-300.
Saitou, M., and Miyauchi, H. (2016). Gametogenesis from Pluripotent Stem Cells. Cell Stem Cell *18*, 721-735.
Sakuma, T., Hosoi, S., Woltjen, K., Suzuki, K., Kashiwagi, K., Wada, H., Ochiai, H., Miyamoto, T., Kawai, N., Sasakura, Y.*, et al.* (2013). Efficient TALEN construction and evaluation methods for human cell and animal applications. Genes Cells *18*, 315-326.
Sasaki, K., Yokobayashi, S., Nakamura, T., Okamoto, I., Yabuta, Y., Kurimoto, K., Ohta, H., Moritoki, Y., Iwatani, C., Tsuchiya, H.*, et al.* (2015). Robust In Vitro Induction of Human Germ Cell Fate from Pluripotent Stem Cells. Cell Stem Cell *17*, 178-194.
Seisenberger, S., Andrews, S., Krueger, F., Arand, J., Walter, J., Santos, F., Popp, C., Thienpont, B., Dean, W., and Reik, W. (2012). The dynamics of genome-wide DNA methylation reprogramming in mouse primordial germ cells. Mol Cell *48*, 849-862.
Seki, Y., Yamaji, M., Yabuta, Y., Sano, M., Shigeta, M., Matsui, Y., Saga, Y., Tachibana, M., Shinkai, Y., and Saitou, M. (2007). Cellular dynamics associated with the genome-wide epigenetic reprogramming in migrating primordial germ cells in mice. Development *134*, 2627-2638.
Shirane, K., Kurimoto, K., Yabuta, Y., Yamaji, M., Satoh, J., Ito, S., Watanabe, A., Hayashi, K., Saitou, M., and Sasaki, H. (2016). Global Landscape and Regulatory Principles of DNA Methylation Reprogramming for Germ Cell Specification by Mouse Pluripotent Stem Cells. Dev Cell *39*, 87-103.
Soh, Y.Q., Junker, J.P., Gill, M.E., Mueller, J.L., van Oudenaarden, A., and Page, D.C. (2015). A Gene Regulatory Program for Meiotic Prophase in the Fetal Ovary. PLoS Genet *11*, e1005531.
Spiller, C.M., and Bowles, J. (2015). Sex determination in mammalian germ cells. Asian J Androl *17*, 427-432.
Taketo, T. (2015). The role of sex chromosomes in mammalian germ cell differentiation: can the germ cells carrying X and Y chromosomes differentiate into fertile oocytes? Asian J Androl *17*, 360-366.
Wu, Q., Fukuda, K., Kato, Y., Zhou, Z., Deng, C.X., and Saga, Y. (2016). Sexual Fate Change of XX Germ Cells Caused by the Deletion of SMAD4 and STRA8 Independent of Somatic Sex Reprogramming. PLoS Biol *14*, e1002553.

Yamashiro, C., Hirota, T., Kurimoto, K., Nakamura, T., Yabuta, Y., Nagaoka, S.I., Ohta, H., Yamamoto, T., and Saitou, M. (2016). Persistent Requirement and Alteration of the Key Targets of PRDM1 During Primordial Germ Cell Development in Mice. Biol Reprod *94*, 7.

Yao, H.H., Matzuk, M.M., Jorgez, C.J., Menke, D.B., Page, D.C., Swain, A., and Capel, B. (2004). Follistatin operates downstream of Wnt4 in mammalian ovary organogenesis. Developmental dynamics : an official publication of the American Association of Anatomists *230*, 210-215.

Ying, Y., and Zhao, G.Q. (2001). Cooperation of endoderm-derived BMP2 and extraembryonic ectoderm-derived BMP4 in primordial germ cell generation in the mouse. Dev Biol *232*, 484-492.

Yuan, L., Liu, J.G., Zhao, J., Brundell, E., Daneholt, B., and Hoog, C. (2000). The murine SCP3 gene is required for synaptonemal complex assembly, chromosome synapsis, and male fertility. Mol Cell *5*, 73-83.

Zamboni, L., and Upadhyay, S. (1983). Germ cell differentiation in mouse adrenal glands. J Exp Zool *228*, 173-193.

Zhang, H., and Bradley, A. (1996). Mice deficient for BMP2 are nonviable and have defects in amnion/chorion and cardiac development. Development *122*, 2977-2986.

FIGURE LEGENDS

Figure 1. A Screening for the Factors Inducing the Female Germ Cell Fate

(A) (left) Scheme for the screening of the factors inducing the female germ-cell fate. d4/c0 PGCLCs [BV (+) cells] induced from BVSCDT (XY) or BVSCVR (XX) ESCs were sorted by FACS onto m220 feeders and cultured with Forskolin (F), Rolipram (R) and SCF (S) (Ohta et al., 2017). Cytokines/chemicals for the screening were provided from c3. (right) Expression of *Dazl* and *Ddx4* in d4 PGCLCs and germ cells from E9.5 to E13.5 (female germ cells at E12.5 and E13.5) measured by RNA-seq (Ohta et al., 2017; Sasaki et al., 2015; Yamashiro et al., 2016). The averages of two replicates are shown.

(B) (left) Scheme for the FACS. The DT levels among BV (+) cells were analyzed at c7. (right) The FACS results for the cultures with the indicated conditions. The number indicates the percentage of DT (+) cells within the indicated gate.

(C) Summary of the results in (B). Red dots indicate conditions with BMPs, while a blue dot represents the control without additional cytokines/chemicals.

(D, E) (left) Representative FACS plots of c9 cells (BVSCVR) under the indicated conditions. The boxed areas [SC (+) cells] in the upper plots were separated with BV and VR in the lower plots. A BVSC plot of E15.5 fetal primary oocytes is shown in (D). (right) Percentage of the VR (+) cells under the indicated conditions. The means and the standard deviations (SDs) of two independent experiments are shown.

(G) DDX4 and SCP3 expression with DAPI in E15.5 fetal oocytes (top) and c9 RAB2 cells [BV/SC (+)] induced from BVSC ESCs (XX) (bottom). Bar, 10 μm.

Figure 2. Induction of the Female Fate in PGCLCs by BMP and RA

(A) Representative FACS plots (top: BVSC expression; bottom: BVVR expression) of the PGCLC culture under the control condition (left), with RA (middle), and with RA and BMP2 (right) at c5, c7, and c9. The SC (+) cells boxed in the top panels were analyzed in the bottom panels, with percentages of cells in the boxed areas indicated.

(B) (left) BVSC fluorescence and (right) SCP3/STRA8/DAZL expression in BV/SC (+) cells during the PGCLC culture with RA and BMP2 at c5, c7, and c9. Bars, 200 μm (left) and 20 μm (right).

(C) The percentages of STRA8 (+) and SCP3 (+) cells among BV/SC (+) cells, based on IF analyses at c5, c7, and c9. The means and the SDs of two independent experiments are shown.

(D) Synchronicity of the entry into the meiotic prophase. The vertical axis indicates the numbers of the colonies counted. The horizontal axis indicates the percentage of SCP3 (+) cells within BV/SC (+) colonies. The colonies consisting of at least 2 cells were counted.

(E) The numbers of BV (+) cells during the control culture and the culture with RA and BMP2. 1,500 BV (+) d4 PGCLCs were seeded at c0. One dot represents the average of 5 replicated culture wells and the bar represents the mean of the dots.

(F) Cell cycle of PGCLCs cultured with RA and BMP2 at c7 and c9 as analyzed by EdU

and 7AAD incorporation.
(G) The progression of meiosis examined by spread analyses of SCP3/γH2AX/SCP1 expression at c9 with RA and BMP2. The percentages of cells at the indicated stages are shown.

Figure 3. Induction of the Female Fate in PGCs by BMP and RA
(A) Scheme of the PGC culture. SG (+) cells were cultured with Forskolin, Rolipram, and SCF on m220 feeders, and RA and/or BMP2 were provided at c0.
(B) DDX4/SCP3/SG expression under the indicated conditions at c4. Bar, 20 μm.
(C) The percentages of SCP3 (+) cells among DDX4 (+) cells. The means and SDs of duplicated wells are shown.
(D) Scheme of the E11.5 fetal ovary culture. BMS493 or LDN1931189 was provided at c0.
(E) DDX4/SCP3 expression under the indicated conditions at c4. Bar, 20 μm.
(F) The percentages of SCP3 (+) cells among DDX4 (+) cells. The means and SDs of two independent experiments are shown.
(G) Scheme of the LDN1931189 administration (every 12 hr) into pregnant mice.
(H) DDX4/SCP3 expression under the indicated conditions at c4. Bar, 20 μm.
(I) The percentages of SCP3 (+) cells among DDX4 (+) cells. The means and SDs in two anterior and two posterior regions of the gonads are shown.

Figure 4. Transcriptome during Female Sex Determination of PGCLCs/PGCs
(A) UHC (Ward method) of the indicated cells using genes with $\log_2(RPM+1) > 2$ in at least one sample (15,849 genes) and a heat map of the expression levels of key genes. ct: cultured PGCLCs without RA or BMP2. The color coding is as indicated.
(B) PCA of germ cells in vivo (E9.5-E11.5 PGCs, E12.5-E15.5 male and female germ cells) and in vitro (cultured PGCLCs). A purple dotted circle clusters PGCs (E9.5, E10.5, E11.5) and PGCLCs (c0, c3). A red dotted circle clusters fetal oocytes (E14.5, E15.5 female germ cells) and c9 RAB2 cells. Blue, red, pink and yellow represent male germ cells, female germ cells, PGCLCs cultured with RA, and PGCLCs cultured with RAB2, respectively.
(C) (top) Scatter plot comparison of gene expressions between E14.5 male and female germ cells (left) and between E14.5 female and E9.5 germ cells (right). Orange, green, red, blue, and grey dots indicate early PGC, late germ-cell, fetal oocyte, PSG, and non-classified genes, respectively.
(bottom, left) A heat map of the expression of early PGC genes (orange), late germ-cell genes (green), fetal oocyte genes (red), and prospermatogonia (PSG) genes (blue) (in total: 1,371 genes) in germ cells in vivo and in vitro as indicated. (bottom, right) GO enrichments (p-values indicated) and key genes for each gene class.
(D) Box plots of the levels of fetal oocyte genes (left) and late germ-cell genes (right) in the indicated cells [the averages (horizontal lines), 25^{th} and 75^{th} percentiles (boxes), and

5th and 95th percentiles (error bars) are shown].
(E) Expression [$\log_2$(RPM+1)] of key genes during female sex determination of PGCLCs/PGCs. The averages of two replicates are shown. Purple, green, and orange filled circles and red open circles represent E9.5 PGC, E14.5 fetal oocytes, c9 RAB2 cells, and c9 RA cells, respectively. The color code of the line above the gene name is the same as in (C).

Figure 5. STRA8 Function in Female Sex Determination
(A) Representative FACS plots (BVSC) of wild-type (WT) and *Stra8*-knockout (SK1) PGCLCs at c3, c5, c7 and c9 with RAB2.
(B) The numbers of SC (+) cells estimated by FACS during the culture as in (A). The initial BV (+) cell numbers (c0) were 5,000. The means and SDs of two independent experiments are shown.
(C) Cell cycle of WT and SK1 PGCLCs cultured under the control condition (top) or with RAB2 (bottom) at c9 as analyzed by EdU and 7AAD incorporation.
(D) PCA of the indicated cells. Arrows highlight differences between the WT and SK1 cells.
(E) The number of DEGs between WT and SK1 cells [$\log_2$(RPM+1) > 4, $\log_2$(fold change) > 2] cultured with RAB2 at c5, c7, and c9.
(F) (top) Scatter-plot comparison of gene expression between WT and SK1 c9 RAB2 cells and selected GO terms for DEGs. Four gene classes are color-coded as indicated. (bottom) Non-DEGs [$\log_2$(fold change) < 1] among fetal oocyte genes or late germ-cell genes between WT and SK1 c9 RAB2 cells and their selected GO terms. 153/476 (~32.1%) and 164/254 (~64.6%) genes are non-DEGs for fetal oocyte genes and late germ-cell genes, respectively.
(G) Box plots of the levels of fetal oocyte genes, late germ-cell genes and RA genes in the indicated cells [the averages (horizontal lines), 25th and 75th percentiles (boxes), and 5th and 95th percentiles (error bars) are shown]. c9_KO: c9 SK1 cells with RAB2; c9_WT, c9 WT cells with RAB2.
(H) Expression [$\log_2$(RPM+1)] of key genes in WT and SK1 cells during the RAB2 culture. The averages of two replicates are shown. The color coding is as indicated.

Figure 6. Competence for the Female Germ Cell Fate
(A) Scheme of the experiments. Ct: control; RB: RAB2 culture for 48 hrs from d4/c0 or c7.
(B) PCA of the indicated cells. Yellow circles with black or red outline represent d4/c0, c0 Ct and c0 RB or c7, c7 Ct and c7 RB cells, respectively. Black or yellow arrowheads indicate cells with Ct or RB culture.
(C) The numbers of DEGs between c0 RB and Ct cultures (left) and between c7 RB and Ct cultures (right).
(D) GO terms for the 218 genes up-regulated in c7 RB cells compared to c7 Ct cells.

(E) Scatter-plot representation of the relationship between expression and promoter-5mC levels in c0 Ct/RB (right) and c7 Ct/RB cells (left). Red and blue circles indicate "meiosis" genes (GO: 0007126) (D), whose % 5mC differences between d4/c0 and c7 PGCLCs are > 20% (42 genes) or < 20% (110 genes), respectively. Red circles with black outlines indicate genes with a $\log_2(RPM+1) > 5$.
(F) Box plots of the levels of "meiosis" genes in the indicated cells [the averages (horizontal lines), 25th and 75th percentiles (boxes), and 5th and 95th percentiles (error bars) are shown]. * indicates a statistical significance [*t*-test (var = T), $p < 0.05$]. The color coding is as in (E).
(G) Scatter-plot representations of the relationship of the expression differences of "meiosis" genes (left) during early-to-late (E9.5 to E11.5) PGC transition with those during d4/c0-to-c7 PGCLC culture, and (right) during late PGC-to-E13.5 female-germ-cell transition with those during c7 to cy RAB2 PGCLC culture. Correlation coefficients are indicated.
(H) PCA of E9.5 PGCs, E11.5 PGCs, E13.5 female and male germ cells, d4/c0PGCLCs, c7PGCLCs and c7 RAB2 PGCLCs based on the "meiosis" gene expression.

Figure 7. Models for the Mechanism of Female Sex Determination in Mouse Germ Cells
(A) A model for the roles of BMP and RA signaling. BMP and RA signaling contribute to the repression of early PGC genes (e.g., *Prdm1, Prdm14*, *Tfap2c*, *Pou5f1, Sox2, Nanog* and *Esrrb*, etc.) and to the up-regulation of late germ-cell genes (e.g., *Ddx4, Dazl, Piwil2, Mov10l1* and *Mael*, etc.) and fetal oocyte genes (e.g., *Stra8*, *Rec8, Sycp3, Hormad1* as meiosis genes, and *Figla, Ybx2, Sohlh2* as oocyte-development genes). With BMP signaling, STRA8 promotes the expression of meiosis genes and inhibits the ectopic expression of developmental genes induced by RA signaling (RA genes). STRA8 does not have a significant impact on late germ-cell genes and oocyte-development genes. Without BMP signaling, STRA8 cannot fully up-regulate meiosis genes or induce meiosis entry. BMP and RA signaling do not up-regulate prospermatogonia genes.
(B) A model of the competence for the female germ-cell fate. The maturation from early-to-late PGCs depends on the intrinsic demethylation of key promoters by proliferation and the differentiation from late PGCs to fetal primary oocytes depends on extrinsic BMP and RA signaling.

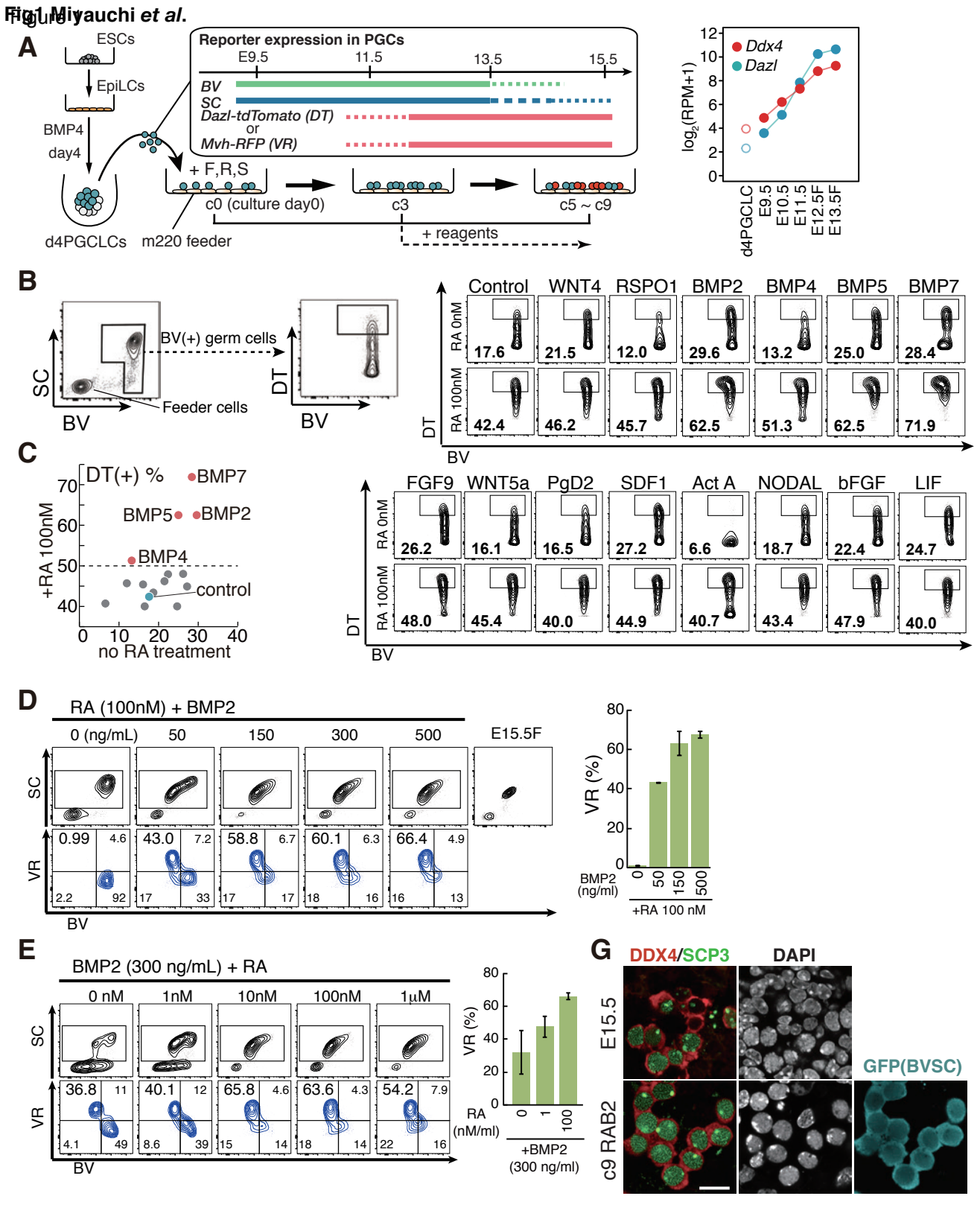
A
ESCs
EpiLCs
BMP4
day4
d4PGCLCs
m220 feeder
+ F,R,S
c0 (culture day0)
c3
c5 ~ c9
+ reagents
Reporter expression in PGCs
E9.5
11.5
13.5
15.5
BV
SC
Dazl-tdTomato (DT)
or
Mvh-RFP (VR)
log2(RPM+1)
Ddx4
Dazl
d4PGCLC
E9.5
E10.5
E11.5
E12.5F
E13.5F
B
SC
BV
BV(+) germ cells
Feeder cells
DT
BV
Control
WNT4
RSPO1
BMP2
BMP4
BMP5
BMP7
RA 0nM
RA 100nM
17.6
21.5
12.0
29.6
13.2
25.0
28.4
42.4
46.2
45.7
62.5
51.3
62.5
71.9
DT
BV
C
DT(+) %
BMP7
BMP5
BMP2
BMP4
control
+RA 100nM
no RA treatment
FGF9
WNT5a
PgD2
SDF1
Act A
NODAL
bFGF
LIF
26.2
16.1
16.5
27.2
6.6
18.7
22.4
24.7
48.0
45.4
40.0
44.9
40.7
43.4
47.9
40.0
D
RA (100nM) + BMP2
0 (ng/mL)
50
150
300
500
E15.5F
SC
VR
BV
0.99
4.6
2.2
92
43.0
7.2
17
33
58.8
6.7
17
17
60.1
6.3
18
16
66.4
4.9
16
13
VR (%)
BMP2 (ng/ml)
+RA 100 nM
E
BMP2 (300 ng/mL) + RA
0 nM
1nM
10nM
100nM
1μM
SC
VR
BV
36.8
11
4.1
49
40.1
12
8.6
39
65.8
4.6
15
14
63.6
4.3
18
14
54.2
7.9
22
16
VR (%)
RA (nM/ml)
+BMP2 (300 ng/ml)
G
DDX4/SCP3
DAPI
E15.5
c9 RAB2
GFP(BVSC)

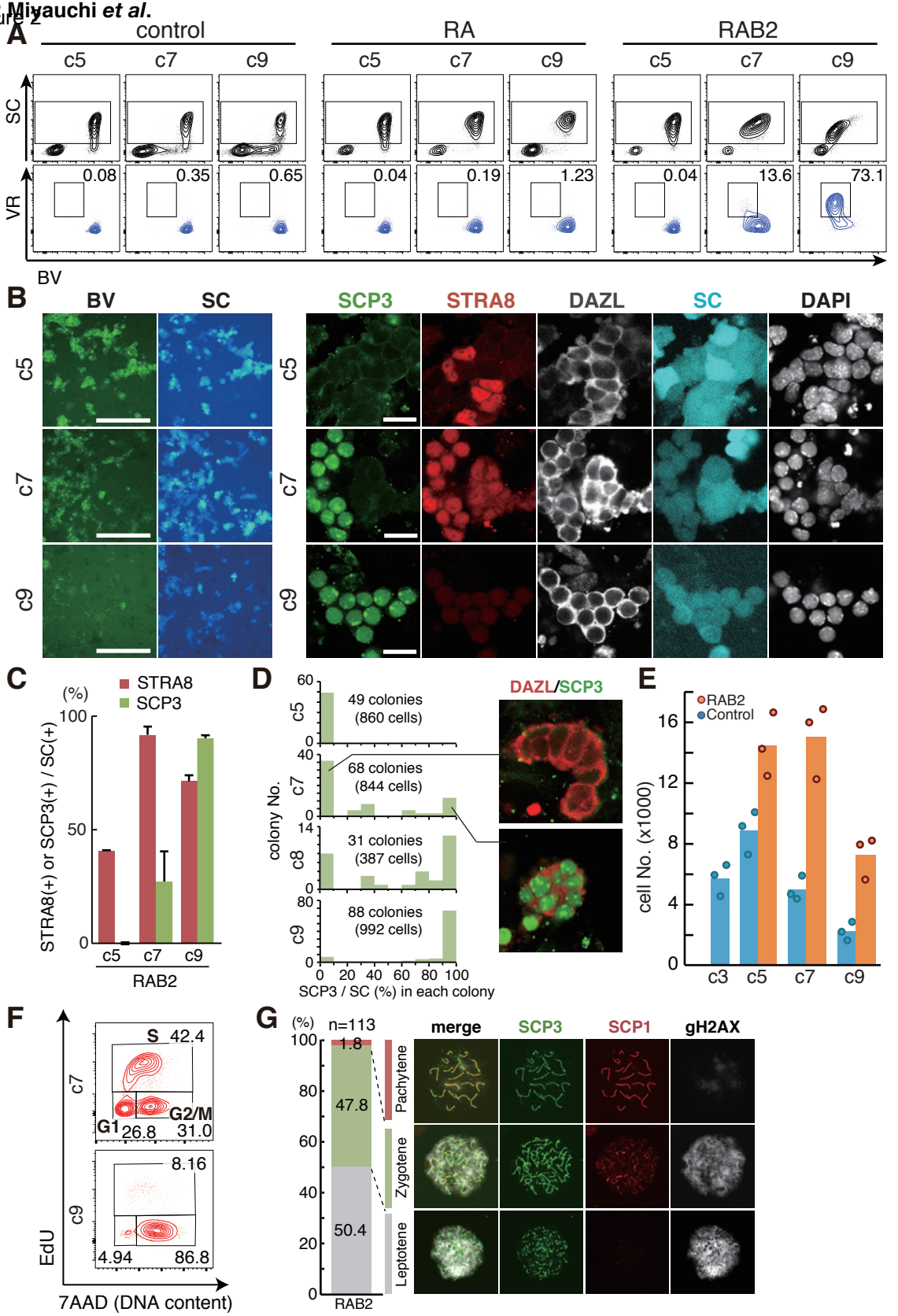
A
control
RA
RAB2
c5
c7
c9
SC
VR
0.08
0.35
0.65
0.04
0.19
1.23
0.04
13.6
73.1
BV
B
BV
SC
SCP3
STRA8
DAZL
SC
DAPI
C
STRA8
SCP3
(%)
STRA8(+) or SCP3(+) / SC(+)
RAB2
D
49 colonies
(860 cells)
68 colonies
(844 cells)
31 colonies
(387 cells)
88 colonies
(992 cells)
colony No.
SCP3 / SC (%) in each colony
DAZL/SCP3
E
RAB2
Control
cell No. (x1000)
c3
c5
c7
c9
F
S 42.4
G2/M
G1 26.8
31.0
8.16
4.94
86.8
EdU
7AAD (DNA content)
G
(%)
n=113
1.8
47.8
50.4
Pachytene
Zygotene
Leptotene
RAB2
merge
SCP3
SCP1
gH2AX

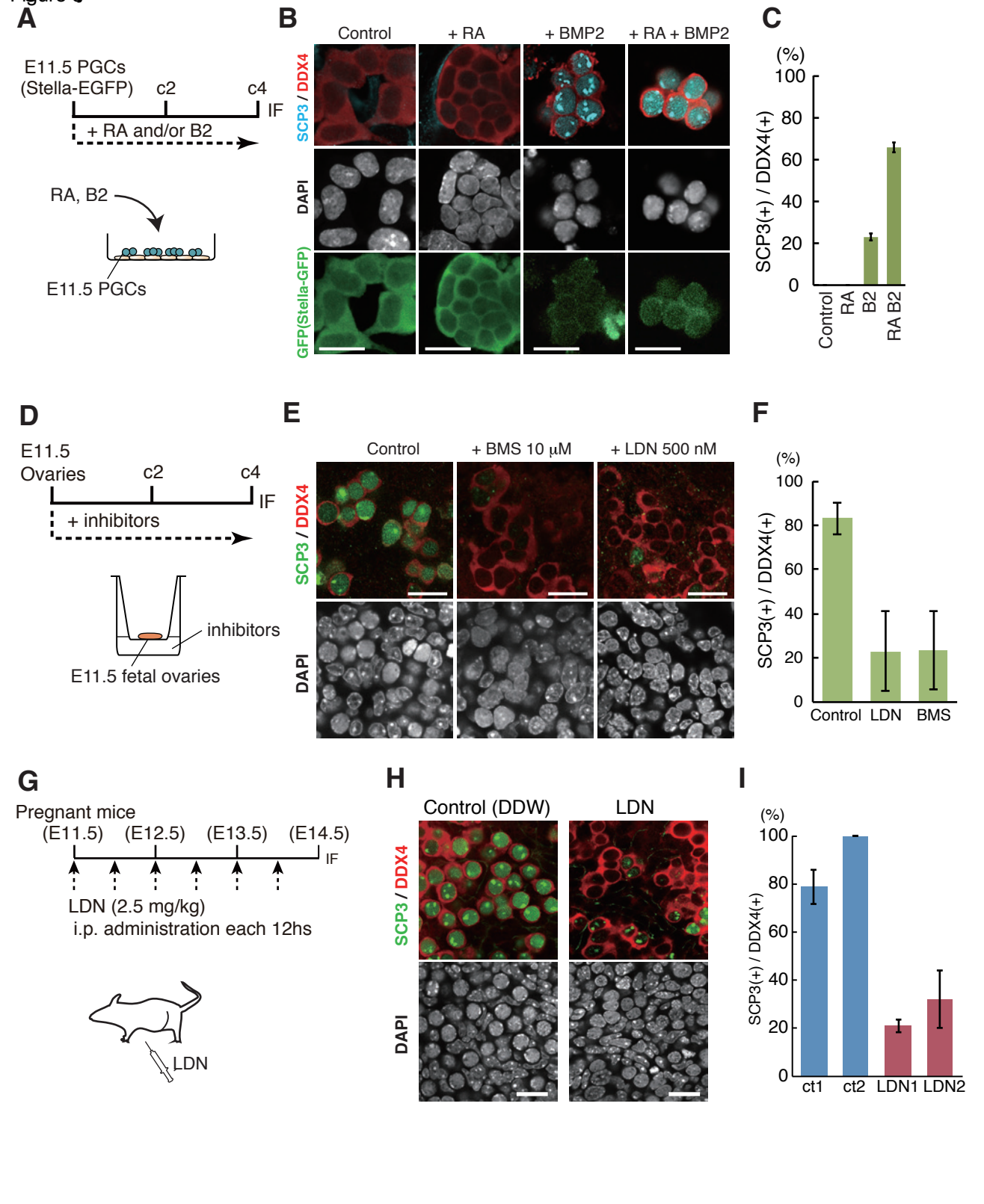
A
E11.5 PGCs
(Stella-EGFP)
c2
c4
IF
+ RA and/or B2
RA, B2
E11.5 PGCs
B
Control
+ RA
+ BMP2
+ RA + BMP2
SCP3 / DDX4
DAPI
GFP(Stella-GFP)
C
(%)
SCP3(+) / DDX4(+)
Control
RA
B2
RA B2
D
E11.5
Ovaries
c2
c4
IF
+ inhibitors
inhibitors
E11.5 fetal ovaries
E
Control
+ BMS 10 μM
+ LDN 500 nM
SCP3 / DDX4
DAPI
F
(%)
SCP3(+) / DDX4(+)
Control
LDN
BMS
G
Pregnant mice
(E11.5)
(E12.5)
(E13.5)
(E14.5)
IF
LDN (2.5 mg/kg)
i.p. administration each 12hs
LDN
H
Control (DDW)
LDN
SCP3 / DDX4
DAPI
I
(%)
SCP3(+) / DDX4(+)
ct1
ct2
LDN1
LDN2

Figure 4 **Fig4 Miyauchi *et al*.**

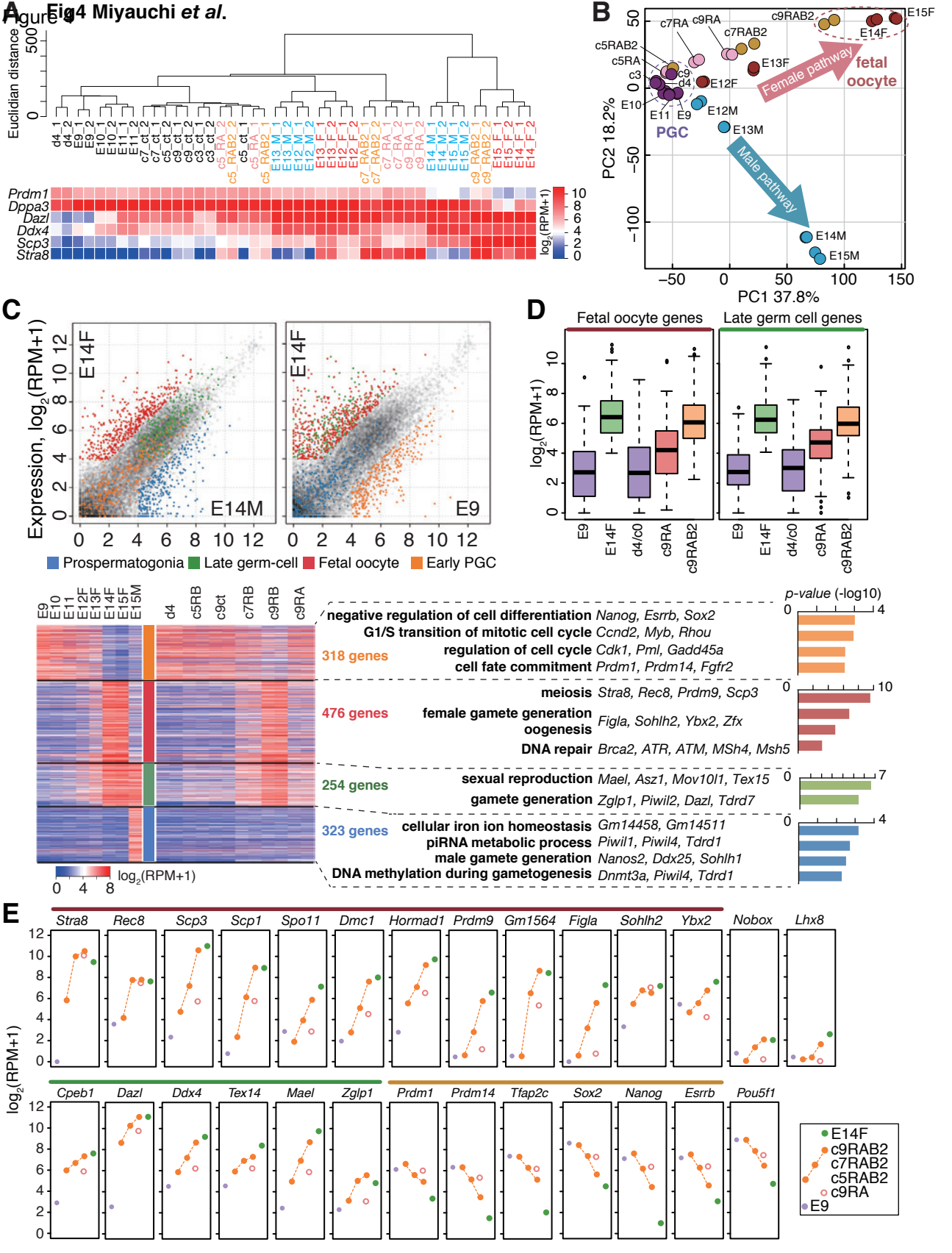

Figure 5

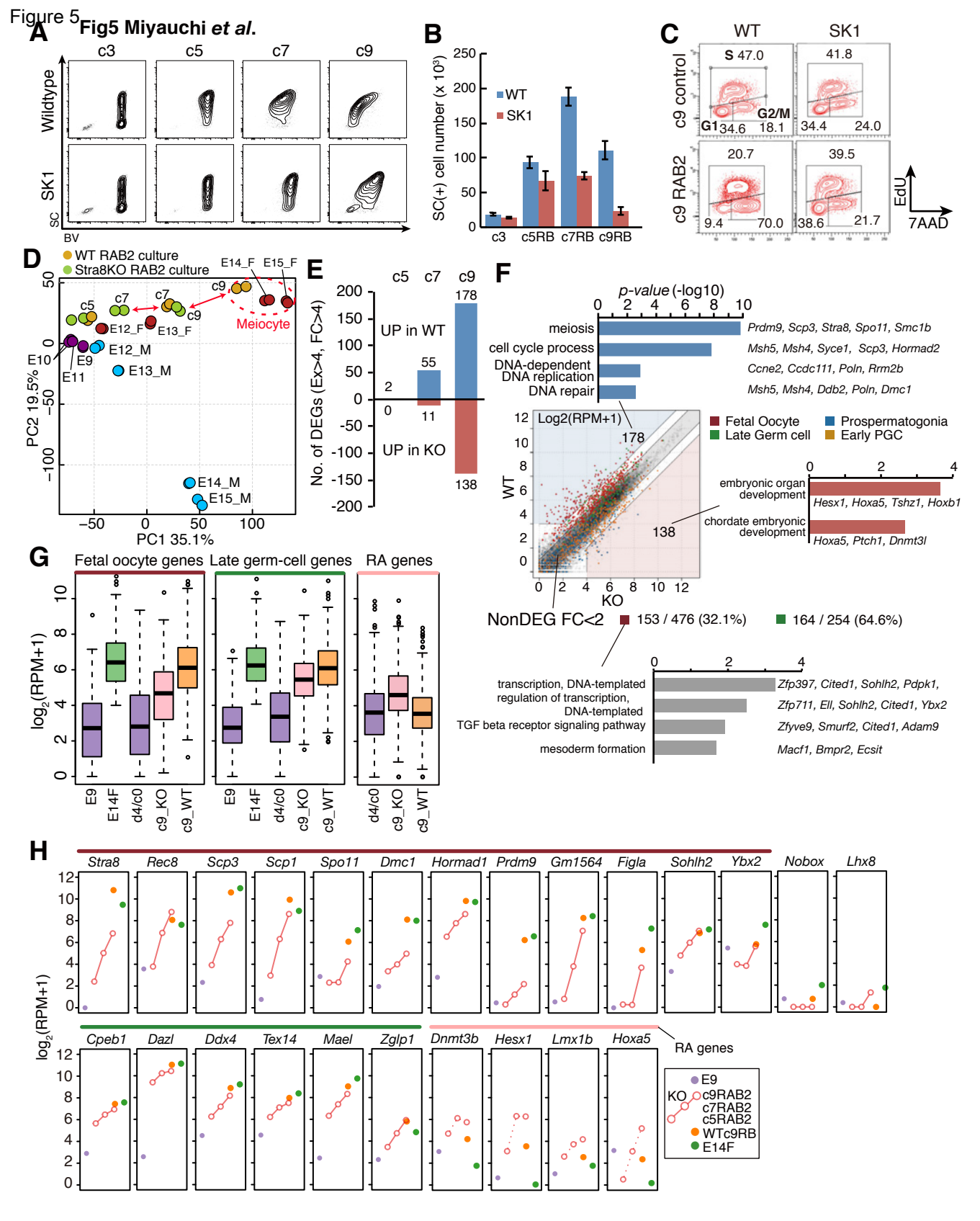
A
Fig5 Miyauchi et al.
c3
c5
c7
c9
Wildtype
SK1
SC
BV
B
SC(+) cell number (x 10³)
WT
SK1
c3
c5RB
c7RB
c9RB
C
WT
SK1
c9 control
c9 RAB2
S 47.0
41.8
G2/M
G1 34.6
18.1
34.4
24.0
20.7
39.5
9.4
70.0
38.6
21.7
EdU
7AAD
D
WT RAB2 culture
Stra8KO RAB2 culture
E14_F
E15_F
c9
c5
c7
c7
c9
Meiocyte
E12_F
E13_F
E10
E9
E11
E12_M
E13_M
E14_M
E15_M
PC2 19.5%
PC1 35.1%
E
c5
c7
c9
178
UP in WT
55
2
0
11
UP in KO
138
No. of DEGs (Ex>4, FC>4)
F
p-value (-log10)
meiosis
cell cycle process
DNA-dependent DNA replication
DNA repair
Prdm9, Scp3, Stra8, Spo11, Smc1b
Msh5, Msh4, Syce1, Scp3, Hormad2
Ccne2, Ccdc111, Poln, Rrm2b
Msh5, Msh4, Ddb2, Poln, Dmc1
Log2(RPM+1)
178
138
WT
KO
Fetal Oocyte
Late Germ cell
Prospermatogonia
Early PGC
embryonic organ development
Hesx1, Hoxa5, Tshz1, Hoxb1
chordate embryonic development
Hoxa5, Ptch1, Dnmt3l
NonDEG FC<2
153 / 476 (32.1%)
164 / 254 (64.6%)
transcription, DNA-templated
regulation of transcription, DNA-templated
TGF beta receptor signaling pathway
mesoderm formation
Zfp397, Cited1, Sohlh2, Pdpk1,
Zfp711, Ell, Sohlh2, Cited1, Ybx2
Zfyve9, Smurf2, Cited1, Adam9
Macf1, Bmpr2, Ecsit
G
Fetal oocyte genes
Late germ-cell genes
RA genes
log2(RPM+1)
E9
E14F
d4/c0
c9_KO
c9_WT
H
Stra8
Rec8
Scp3
Scp1
Spo11
Dmc1
Hormad1
Prdm9
Gm1564
Figla
Sohlh2
Ybx2
Nobox
Lhx8
Cpeb1
Dazl
Ddx4
Tex14
Mael
Zglp1
Dnmt3b
Hesx1
Lmx1b
Hoxa5
RA genes
log2(RPM+1)
E9
KO
c9RAB2
c7RAB2
c5RAB2
WTc9RB
E14F

Figure 6
Fig6 Miyauchi *et al*.

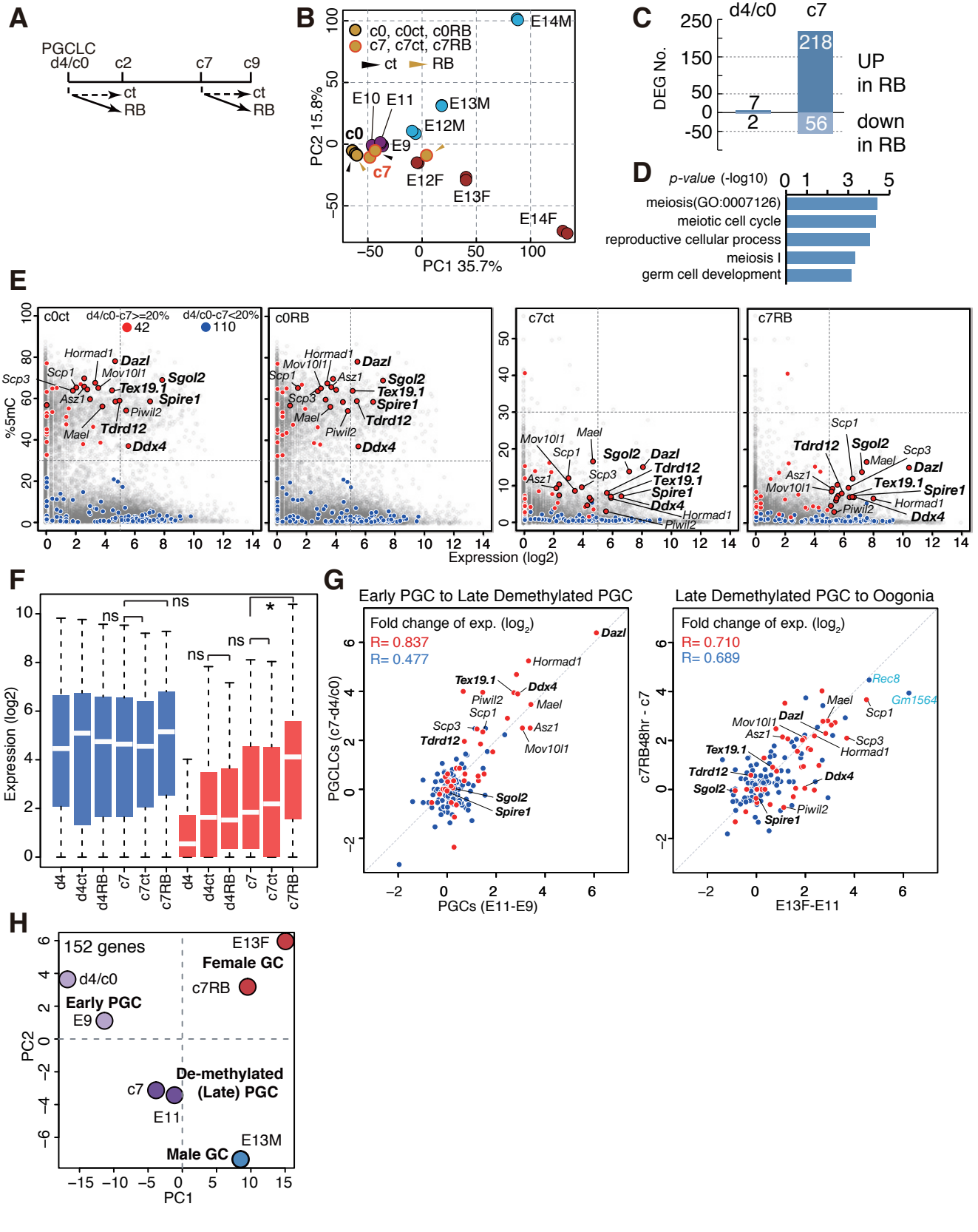

Figure 7
Fig7 Miyauchi *et al*.

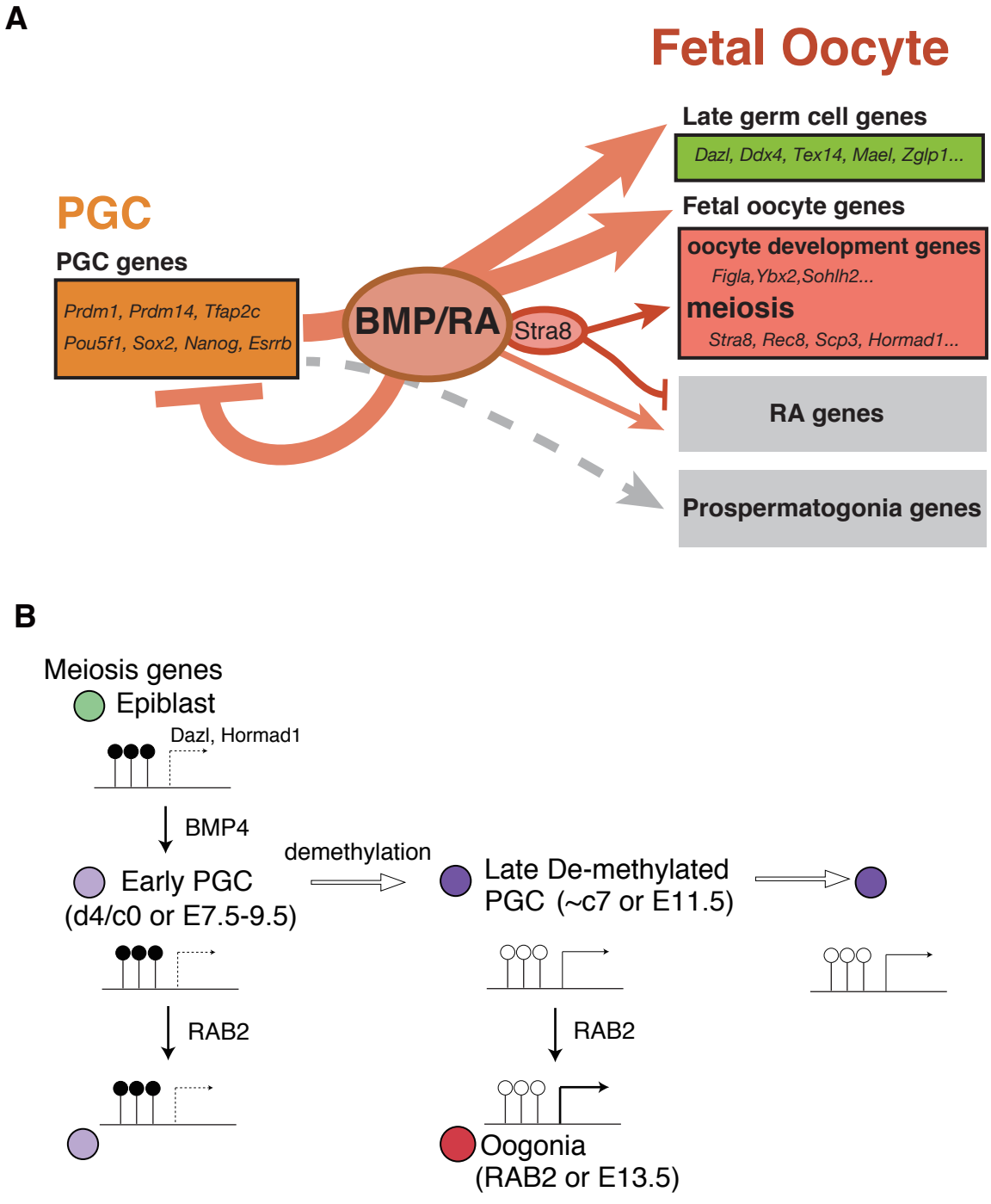

Inventory of Supplemental Information

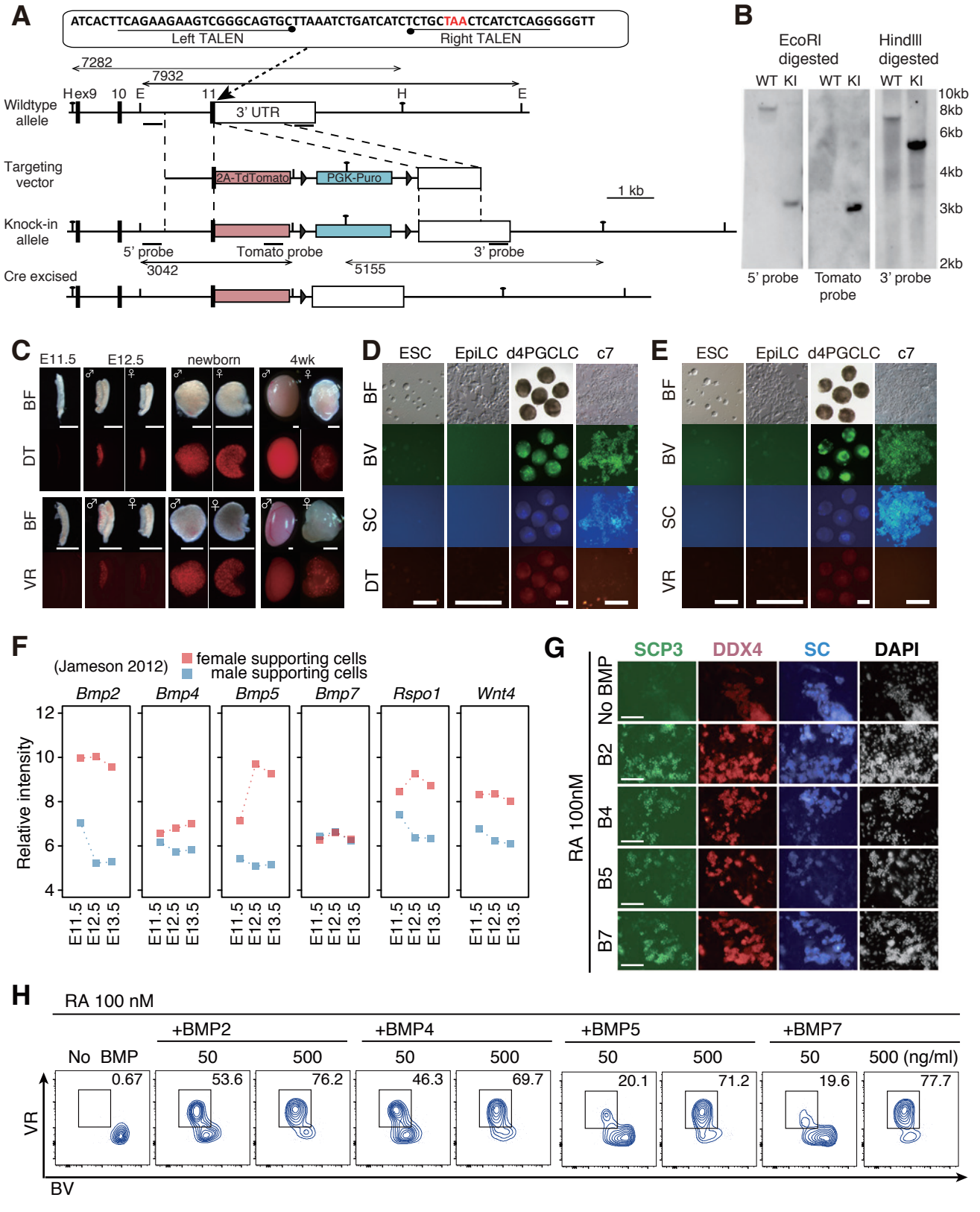
A
ATCACTTCAGAAGAAGTCGGGCAGTGCTTAAATCTGATCATCTCTGCTAACTCATCTCAGGGGGTT
Left TALEN
Right TALEN
7282
7932
Hex9
10
E
11
H
E
Wildtype allele
3' UTR
Targeting vector
2A-TdTomato
PGK-Puro
1 kb
Knock-in allele
5' probe
Tomato probe
3' probe
3042
5155
Cre excised
B
EcoRI digested
HindIII digested
WT KI
WT KI
WT KI
10kb
8kb
6kb
4kb
3kb
2kb
5' probe
Tomato probe
3' probe
C
E11.5
E12.5
newborn
4wk
BF
DT
BF
VR
D
ESC
EpiLC
d4PGCLC
c7
BF
BV
SC
DT
E
ESC
EpiLC
d4PGCLC
c7
BF
BV
SC
VR
F
(Jameson 2012)
female supporting cells
male supporting cells
Bmp2
Bmp4
Bmp5
Bmp7
Rspo1
Wnt4
Relative intensity
12
10
8
6
4
E11.5
E12.5
E13.5
G
SCP3
DDX4
SC
DAPI
No BMP
B2
B4
B5
B7
RA 100nM
H
RA 100 nM
+BMP2
+BMP4
+BMP5
+BMP7
No BMP
50
500
50
500
50
500
50
500 (ng/ml)
0.67
53.6
76.2
46.3
69.7
20.1
71.2
19.6
77.7
VR
BV

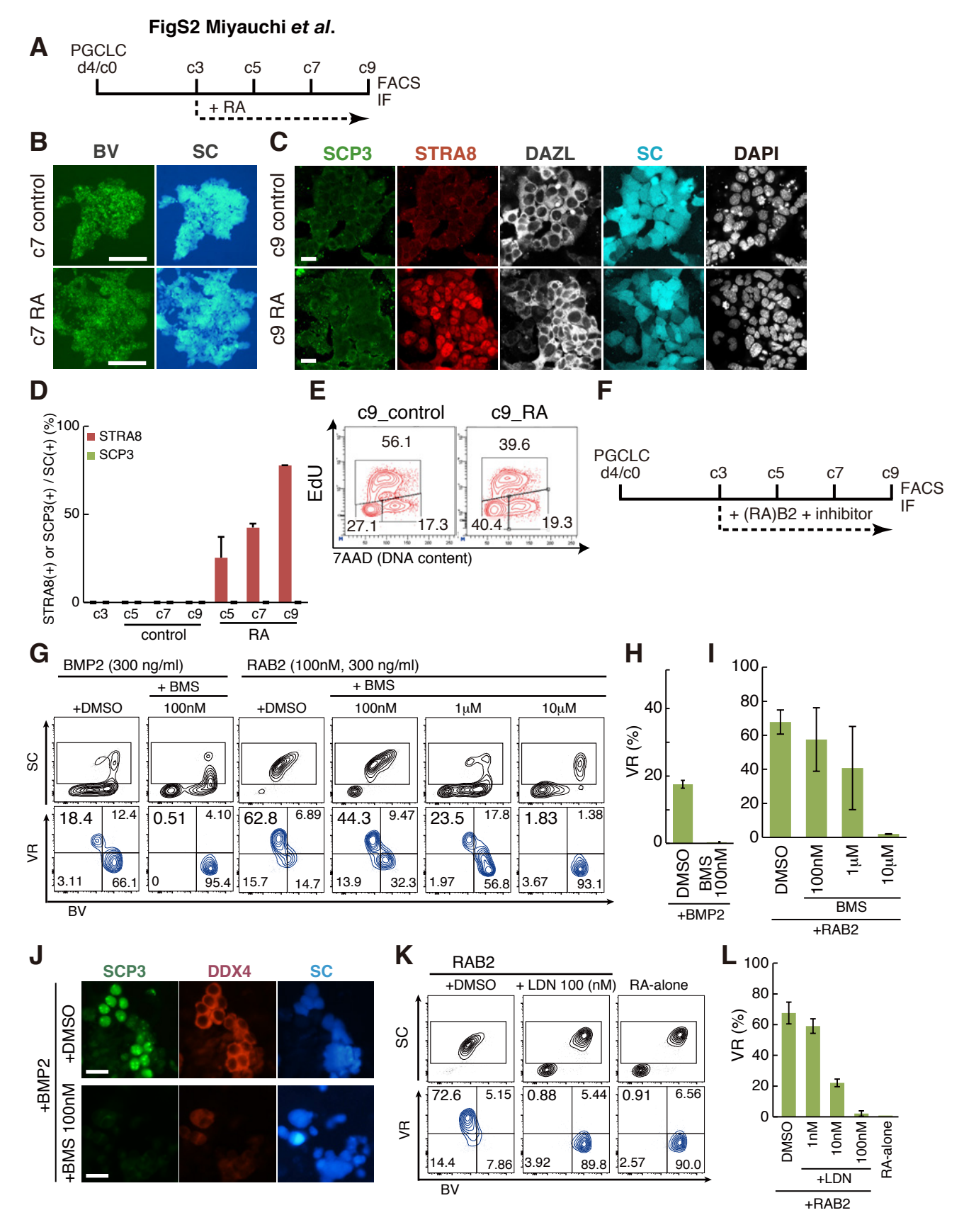
FigS2 Miyauchi et al.
A
PGCLC
d4/c0
c3
c5
c7
c9
FACS
IF
+ RA
B
BV
SC
c7 control
c7 RA
C
SCP3
STRA8
DAZL
SC
DAPI
c9 control
c9 RA
D
STRA8
SCP3
STRA8(+) or SCP3(+) / SC(+) (%)
100
50
0
c3
c5
c7
c9
c5
c7
c9
control
RA
E
c9_control
c9_RA
56.1
39.6
27.1
17.3
40.4
19.3
EdU
7AAD (DNA content)
F
PGCLC
d4/c0
c3
c5
c7
c9
FACS
IF
+ (RA)B2 + inhibitor
G
BMP2 (300 ng/ml)
RAB2 (100nM, 300 ng/ml)
+ BMS
+ BMS
+DMSO
100nM
+DMSO
100nM
1μM
10μM
SC
VR
BV
18.4
12.4
3.11
66.1
0.51
4.10
0
95.4
62.8
6.89
15.7
14.7
44.3
9.47
13.9
32.3
23.5
17.8
1.97
56.8
1.83
1.38
3.67
93.1
H
VR (%)
40
20
0
DMSO
BMS 100nM
+BMP2
I
100
80
60
40
20
0
DMSO
100nM
1μM
10μM
BMS
+RAB2
J
SCP3
DDX4
SC
+BMP2
+DMSO
+BMS 100nM
K
RAB2
+DMSO
+ LDN 100 (nM)
RA-alone
SC
VR
BV
72.6
5.15
14.4
7.86
0.88
5.44
3.92
89.8
0.91
6.56
2.57
90.0
L
VR (%)
100
80
60
40
20
0
DMSO
1nM
10nM
100nM
RA-alone
+LDN
+RAB2

FigS3 Miyauchi *et al*.

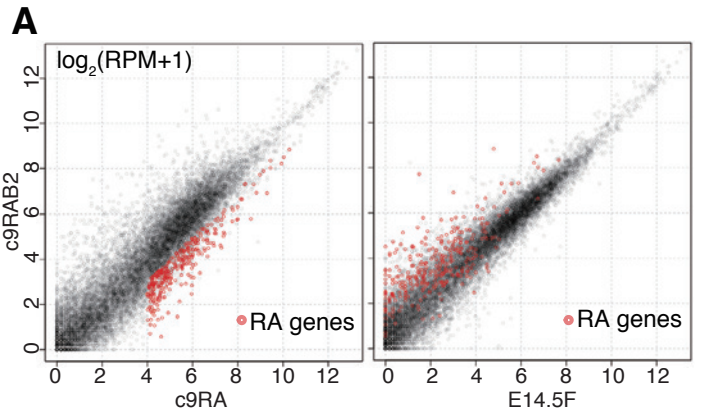

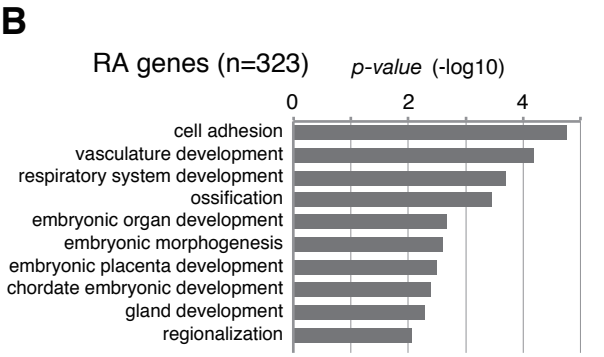

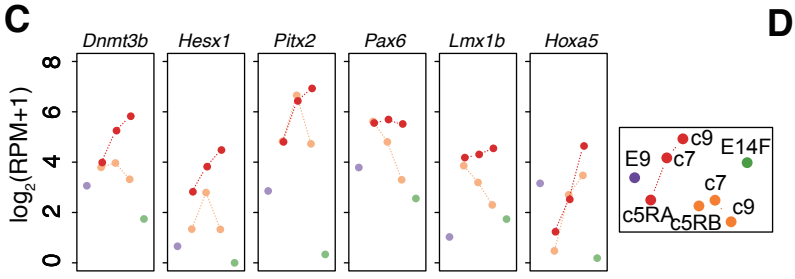

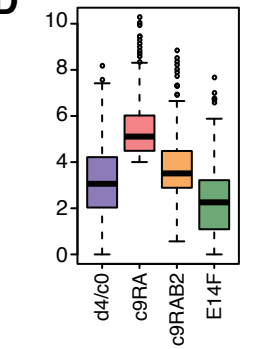

FigS4 Miyauchi *et al*.

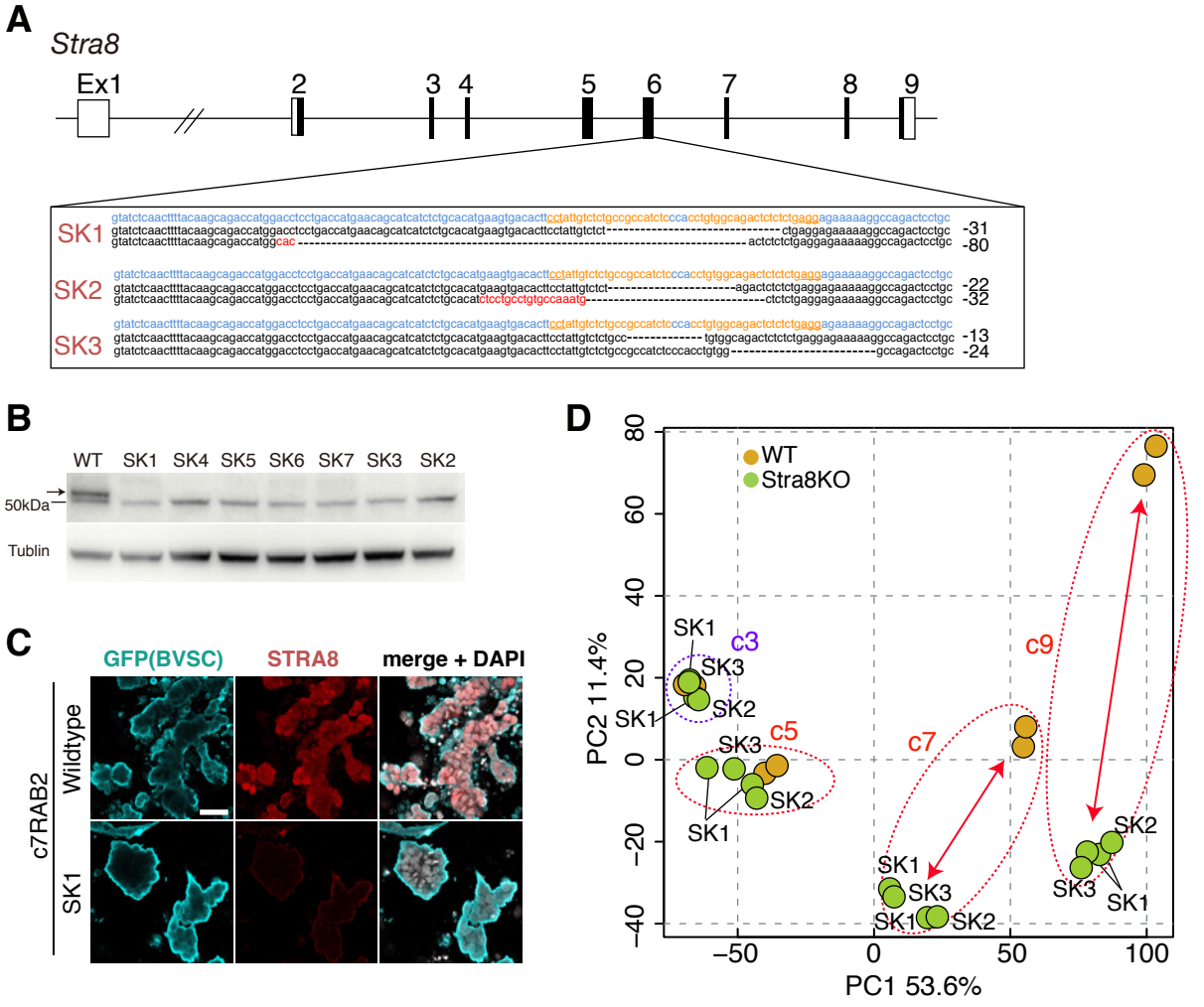

FigS5 Miyauchi *et al*.

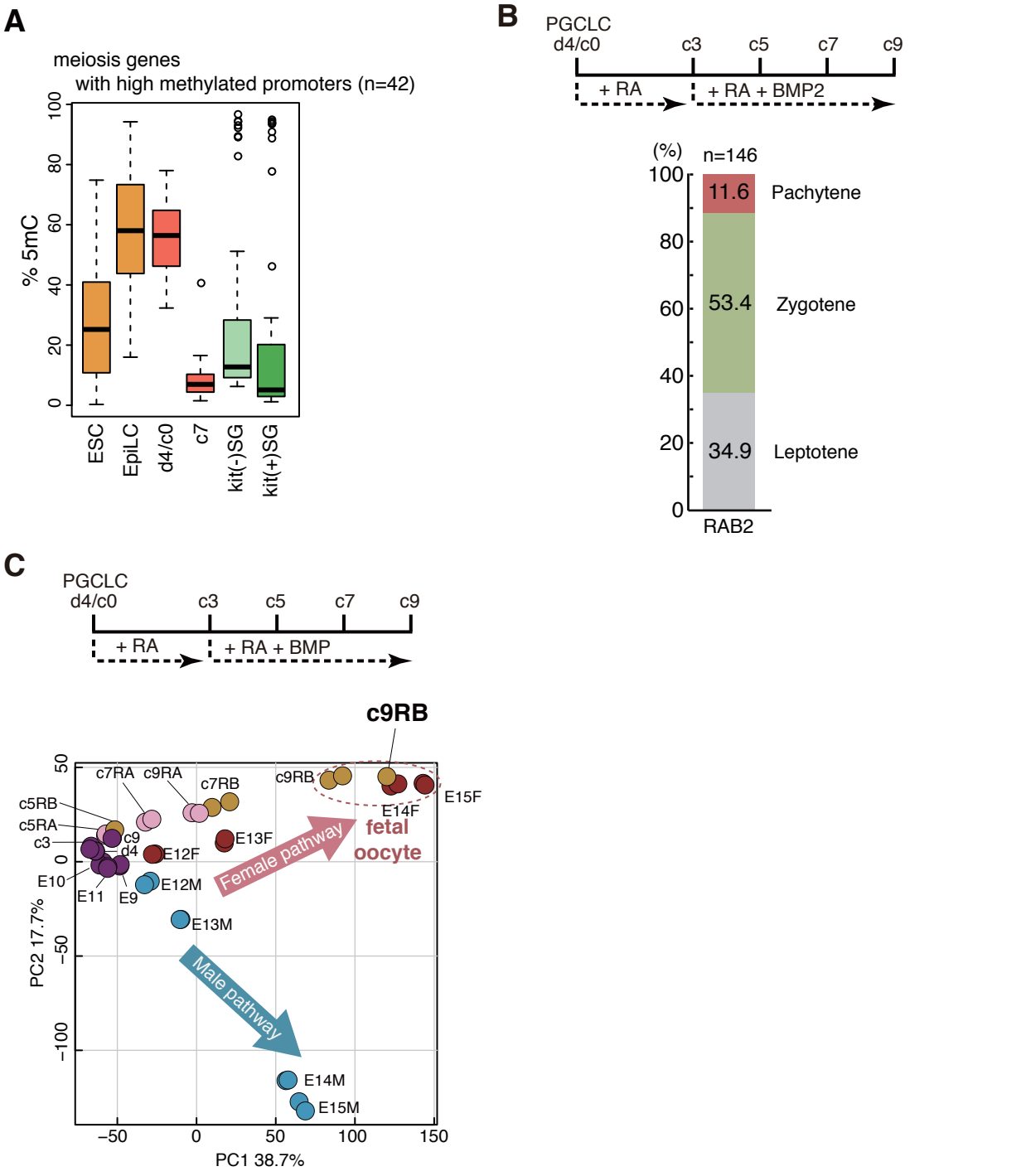

SUPPLEMENTARY FIGURE LEGENDS

Figure S1. BVSCDT/BVSCVR Reporters and the Roles of BMP Ligands in the Induction of Female Germ Cell Fate, Related to Figure 1 and 2.

(A) The targeting strategy to create a *Dazl-tdTomato* (DT) reporter using the TALEN system (Sakuma et al., 2013). H: HindIII site; E: EcoRI site.

(B) Southern blot analysis of the BVSCDT ESCs. The correct targeting was verified using the 5'-, 3'-, and *tdTomato* probes. WT: parental wild-type cells; KI: BVSCDT knockin ESCs.

(C) DT and VR expression in germ cells at the indicated developmental stages. BF: bright field images. Bar, 800 μm.

(D, E) Bright field and fluorescence images of BVSCDT (left) or BVSCVR (right) expression during PGCLC induction and culture. Note that DT and VR are expressed at low levels/not expressed in d4 and c7 PGCLCs. Bar, 200 μm.

(F) Re-analysis of the expression of *Bmps*, *Rspo1*, and *Wnt4* in male and female supporting cells (granulosa cells in female and Sertoli cells in male) reported in (Jameson et al., 2012). The average values from three replicates are shown.

(G) SCP3 and DDX4 expression in c9 BV/SC (+) cells cultured with the indicated BMPs and RA. Bar, 100 μm.

(H) Representative FACS plots for BVVR expression in c9 SC (+) cells cultured with the indicated BMPs (50 or 500 ng/ml) and RA (100 nM). Boxed areas indicate VR (+) cells and their percentages are shown.

Figure S2. RA is Insufficient for Female Sex Determination of PGCLCs, Related to Figure 1 and 2.

(A) Scheme for the experiments in (B-E).

(B, C) BVSC fluorescence (B) and IF images for SCP3, STRA8, DAZL and BV/SC (C) of c7 (B) or c9 (C) cells cultured without (control) or with RA. Bars, 200 μm in (B) and 20 μm in (C).

(D) The percentages of STRA8 (+) and SYCP3 (+) cells among BV/SC (+) cells.

(E) Cell cycle analysis by EdU assay. FACS plots of c9 PGCLCs cultured with or without RA are shown.

Cell cycle of c9 PGCLCs and c9 RA cells analyzed by EdU and 7AAD incorporation.

(F) Scheme for the experiments in (G-L).

(G) Representative BVSC (top) or BVVR (bottom) FACS plots of c9 cells cultured under the indicated conditions. SC (+) cells [boxed cells in the top panels] were analyzed in the bottom panels. The percentages of cells plotted in each quadrant are indicated in the bottom panels.

(H, I) The percentages of the VR (+) cells under the indicated conditions. The means and SDs of two independent experiments are shown.

(J) SCP3 and DDX4 expression in c9 BV/SC (+) cells cultured under the indicated conditions. Bars, 20 μm.

(K) Representative BVSC (top) or BVVR (bottom) FACS plots of c9 cells cultured under the indicated conditions. SC (+) cells [boxed cells in the top panels] were analyzed in the bottom panels. The percentages of cells plotted in each quadrant are indicated in the bottom panels.
(L) The percentages of the VR (+) cells under the indicated conditions. The means and SDs of two independent experiments are shown.

Figure S3. RA Induces Ectopic Developmental Genes, Related to Figure 4.
(A) Scatter plot comparisons of gene expression (left) between c9 RAB2 cells and c9 RA cells, or (right) between c9 RAB2 cells and E14.5 primary oocytes. The ectopic RA genes (323 genes: $\log_2(RPM+1) > 4$; $\log_2$ fold-change: c9 RA – c9 RAB2 > 1) are shown in red.
(B) GO enrichments in the RA genes. *p*-values are indicated.
(C) Expression [$\log_2(RPM+1)$] of selected RA genes in the indicated cells (the color coding is as indicated).
(D) Box plots of the levels of the RA genes in the indicated cells [the averages (horizontal lines), 25^{th} and 75^{th} percentiles (boxes), and 5^{th} and 95^{th} percentiles (error bars) are shown].

Figure S4. Generation of the *Stra8*-knockout (SK) ESCs, Related to Figure 5.
(A) Generation of three independent *Stra8*-knockout ESCs (SK1, 2, 3) by disrupting the exon 6 by CRISPR. The parental line was BDF1-2-1 BVSC ESCs (XY). Nucleotides colored in blue, orange and red indicate wild-type sequences, guide RNA regions for the CRISPR and the insertion mutations, respectively. The deleted regions are indicated by hyphens. The numbers on the right indicate the deleted base numbers.
(B) Western blot analysis of STRA8 expression in wild-type (WT) and *Stra8*-knockout (SK) lines. The upper band indicated by an arrow corresponds to STRA8 and the lower band is a non-specific signal. αTUBULIN was used as a loading control.
(C) Validation of the loss of STRA8 expression in c7 RAB2 BV/SC (+) SK1 cells. Bar, 40 μm.
(D) PCA of the WT and SK1, 2, and 3 RAB2 cells at c3, c5, c7 and c9. Dotted circles represent samples under the same culture periods. Arrows highlight the differences between the WT and SK cells.

Figure S5. Dynamics of the Promoter Methylation Levels of Meiosis Genes and an Enhanced Differentiation Scheme along the Female Germ Cell Pathway, Related to Figure 2, 4, and 6.
(A) Box plots of the 5mC levels of the promoters for the "meiosis" genes with 5mC-level changes > 20% during PGCLC culture (42 genes) in the indicated cells [the averages (horizontal lines), 25^{th} and 75^{th} percentiles (boxes), and 5^{th} and 95^{th} percentiles (error bars) are shown] (Kubo et al., 2015; Ohta et al., 2017; Shirane et al., 2016). SG:

spermatogonia.
(B) (top) Scheme for a modified culture for the induction of the female germ-cell fate. RA was provided from c0 and BMP2 was provided from c3. (bottom) The progression of meiosis examined by spread analyses of SCP3/γH2AX/SCP1 expression at c9 with the protocol shown (top). The percentages of cells at the indicated stages are shown.
(C) (top) Scheme for the modified culture as in (B). (bottom) PCA of the indicated cells. Note that c9 RB cells cultured in the modified scheme are clustered very closely with E14.5 fetal oocytes.

SUPPLEMENTARY TABLES, see separate Excel documents

Table S1. Lists of Early PGC, Late Germ-cell, Fetal Oocyte, PSG, and RA Genes, and Their GO Terms, Related to Figure 4.

Table S2. Lists of DEGs and non-DEGs between Wild-type and *Stra8* Knockout c9 cells, Related to Figure 5.

Table S3. Lists of DEGs between d4/c0 or c7 RAB2 Cells and Their Controls, and of Genes for "Meiosis", Related to Figure 6.

SUPPLEMENTARY REFERENCES

Jameson, S.A., Natarajan, A., Cool, J., DeFalco, T., Maatouk, D.M., Mork, L., Munger, S.C., and Capel, B. (2012). Temporal transcriptional profiling of somatic and germ cells reveals biased lineage priming of sexual fate in the fetal mouse gonad. PLoS Genet *8*, e1002575.

Kubo, N., Toh, H., Shirane, K., Shirakawa, T., Kobayashi, H., Sato, T., Sone, H., Sato, Y., Tomizawa, S., Tsurusaki, Y.*, et al.* (2015). DNA methylation and gene expression dynamics during spermatogonial stem cell differentiation in the early postnatal mouse testis. BMC Genomics *16*, 624.

Ohta, H., Kurimoto, K., Okamoto, I., Nakamura, T., Yabuta, Y., Miyauchi, H., Yamamoto, T., Okuno, Y., Hagiwara, M., Shirane, K.*, et al.* (2017). Expansion of mouse primordial germ cell-like cells in culture reconstitutes an epigenetic blank slate. EMBO J *Under Revision*.

Sakuma, T., Hosoi, S., Woltjen, K., Suzuki, K., Kashiwagi, K., Wada, H., Ochiai, H., Miyamoto, T., Kawai, N., Sasakura, Y.*, et al.* (2013). Efficient TALEN construction and evaluation methods for human cell and animal applications. Genes Cells *18*, 315-326.

Shirane, K., Kurimoto, K., Yabuta, Y., Yamaji, M., Satoh, J., Ito, S., Watanabe, A., Hayashi, K., Saitou, M., and Sasaki, H. (2016). Global Landscape and Regulatory Principles of DNA Methylation Reprogramming for Germ Cell Specification by Mouse Pluripotent Stem Cells. Dev Cell *39*, 87-103.

Supplemental Table S1

Supplemental Table S2

Click here to access/download

Supplemental Movies & Spreadsheets

Table S2.xlsx

Click here to access/download

Supplemental Movies & Spreadsheets

Table S3.xlsx